Adv Polym Sci (2006) 200: 169–208
DOI 10.1007/12_014

Published online: 6 December 2005

Organic and Macromolecular Films and Assemblies as (Bio)reactive Platforms: From Model Studies on Structure–Reactivity Relationships to Submicrometer Patterning

Holger Schönherr (✉) · Geerten H. Degenhart · Barbara Dordi · Chuan Liang Feng · Dorota I. Rozkiewicz · Alexander Shovsky · G. Julius Vancso

MESA$^+$ Institute for Nanotechnology and Faculty of Science and Technology, Department of Materials Science and Technology of Polymers, University of Twente, Postbus 217, 7500 AE Enschede, The Netherlands
h.schonherr@tnw.utwente.nl, g.j.vancso@tnw.utwente.nl

Abstract In this contribution we review our recent progress in studies that aim at the understanding of the relationship between structure and surface reactivity of organic thin films on the one hand, and at the micro- and nanofabrication of bioreactive or biocompatible platforms on the other hand. Self-assembled monolayers (SAMs) of *n*,*n*′-

dithiobis(*N*-hydroxysuccinimidyl-*n*-alkanoate) exposing NHS reactive ester groups were studied as model systems for immobilization reactions of DNA, proteins, and receptors. Reaction kinetics and activation energies were determined quantitatively at length scales ranging from millimeters down to nanometers using, for example, surface infrared spectroscopy and in situ inverted chemical force microscopy (iCFM), respectively. The increase in conformational order with increasing alkane segment length was found to result in reduced reactivity due to steric crowding. This drawback of highly organized monolayer architectures and the inherently limited loading can be circumvented by utilizing well-defined macromolecular thin films. Using amine-terminated polyamidoamine (PAMAM) dendrimers immobilized via soft lithography, as well as scanning probe lithography (SPL) approaches (dip-pen nanolithography, DPN) on NHS ester surfaces, robust micrometer and submicrometer patterned (bio)reactive surfaces, which allow one to achieve high molecular loading in coupling reactions for chip-based assays and sensor surfaces, were fabricated. Covalent coupling afforded the required robustness of the patterned assemblies. Finally, we address micro- and nanopatterned bilayer-based systems. SPL was applied in order to fabricate nanoscale biocompatible supramolecular architectures on solid supports. The adsorption of vesicles onto lipid bilayers was spatially controlled and directed in situ with nanometer-scale precision using SPL. This methodology, which provides a platform for research on proteins incorporated in the lipid bilayers comprising the vesicles, does not require that the vesicles are chemically labeled in order to guide their deposition.

Keywords Biointerfacing · Micropatterning · Nanopatterning · Polymer thin films · Surface reactivity

Abbreviations

SAM	Self-assembled monolayer
NSA	Nonspecific adsorption
NHS	*N*-Hydroxysuccinimide
PNHSMA	Poly(*N*-hydroxysuccinimidyl) methacrylate
CFM	Chemical force microscopy
iCFM	Inverted chemical force microscopy
PAMAM	Polyamidoamine
Gn	Generation *n*
SPL	Scanning probe lithography
AFM	Atomic force microscopy
DPN	Dip-pen nanolithography
μCP	Microcontact printing
2D	Two-dimensional
3D	Three-dimensional
PEG	Poly(ethylene glycol)
DMPC	1,2-Dimyristoyl-*sn*-glycero-3-phosphatidylcholine
SIMS	Secondary ion mass spectrometry
MALDI-MS	Matrix-assisted laser desorption/ionization mass spectrometry
XPS	X-ray photoelectron spectroscopy
ESCA	Electron spectroscopy for chemical analysis
GIR	Grazing incidence reflection
FTIR	Fourier transform infrared
CA	Contact angle

ODT	Octadecanethiol
JKR	Johnson-Kendall-Roberts
x	Extent of reaction
A_t	Integrated absorbance of IR active band at time t
t	Time
θ_i	Contact angle of SAM exposing group i
χ_i	Surface coverage of component in SAM
$\tau_{1/2}$	Half-life of reaction
F	Force
$F_{\text{pull-off}}$	Pull-off force
W_{12}	Work of adhesion
A	Pre-exponential (Arrhenius) factor
E_a	Activation energy
R	Gas constant
T	Absolute temperature
k_b	Boltzmann constant
h	Planck's constant
$\Delta S^{\ddagger}$	Activation entropy
γ_i	Surface free energy of component i
k	Rate constant
k'	First order or pseudo first order rate constant
k''	Second order rate constant
θ	Normalized surface coverage

1 Introduction: Bioreactive Thin Film Architectures and Patterning Methods

The ability to control and modify the chemical and structural properties of surfaces is crucial to advancements in many areas, including selective and environmentally friendly catalysis [1], electronics [2], (bio)chemical sensing [3–8], and biochemistry [9]. Studies of chemical reactions of surfaces may also provide new routes to tailored surface properties. Such surface reactions allow, for example, the tethering of biologically or biomedically important molecules to surfaces, which has significant importance in chemical biology and microarray technology [10–13]. Many approaches rely on monomolecular or thin organic films to covalently couple active species, such as receptors or protein-repellent polymers, to solid supports [14–18]. In addition, owing to increasing surface-to-volume ratios, chemical reactions that occur on organic or polymeric surfaces play a crucial role in many applications, ranging from the previously mentioned array technologies to nanoclusters [19], nanoreactors [20] and drug delivery [21].

Self-assembled monolayers (SAMs) [22–25] are perhaps the most popular model systems for studying chemistry at interfaces under controlled conditions. In the last decade, countless studies have been performed that in-

volve the chemical modification of monolayers [26–35]. However, systematic studies that aim at unraveling important parameters, such as activation energies, have been scarce. In general, it has been noted that the reactivity of functional groups placed in an ordered monolayer environment will be influenced by many factors, such as solvent, steric and electronic effects [36, 37]. Consequently, chemical reactivity can be affected by confinement in highly ordered architectures, which leads (except in rare cases [38]) to reduced reactivity and incomplete conversions [39–42]. For typical applications in, say, the field of sensing, however, rapid reactions and full conversion are desirable to optimize throughput and to minimize reaction times. Similarly, optimal adsorbate orientation and (bio)availability of the active components must be ensured [43].

Since they are intrinsically two-dimensional (2D) systems, SAMs are limited in terms of the surface density of coupled (bio)molecules. The area requirement for SAMs of alkanethiols on gold is $\sim 20–25$ Å^2/molecule, which corresponds to coverages of $5–4 \times 10^{14}$ molecules/cm^2 [44–46]. Hence approaches that extend the dimensionality have received attention. In addition, applications involving biomolecules, such as proteins, may possess stringent constraints to prevent nonspecific adsorption (NSA). Among the various successful approaches to suppressing NSA, the use of or the modification ofsurfaces with poly(ethylene glycol) (PEG) have received most attention [47–50]. Alternative approaches include surface modification with hyperbranched polyglycerines [51] and other SAM termini [52, 53].

The surface coverage achieved in PEG immobilization determines the NSA of proteins as well as cell adhesion [54–57]. Thus, precise control of the modification reactions is also desirable also in this context. This control is directly linked to the detailed study of the relevant surface reactions, and in particular to a fundamental understanding of the relation of structure, local order, local surface properties on the one hand to the reaction kinetics, the activation energies and transition state parameters on the other hand. As previously mentioned, systematic studies of such confined reactions on solid supports have been scarce to date [36, 37, 58]. In particular, the direct assessment of the relation of local, nanometer-scale structure and surface properties to chemical reactivity in wet chemical surface reactions has been hampered by instrumental and analytical limitations so far.

Our target is to ultimately fabricate reactive micro- and nanopatterns for the area-selective immobilization of biologically relevant molecules via covalent coupling. In addition to full control of reactivity and pattern sizes, biocompatibility and minimized NSA are important for rendering these systems useful as generic platforms. In this context we review in this contribution our recent efforts in this area. We focus in particular on (1) the elucidation of structure–reactivity relationships, (2) the in situ compositional analysis of wet chemical reactions in monolayer-based systems down to nanometer length scales, and on (3) the application and refinement of various micro- and

nanofabrication methods to obtain patterns where we have control over the surface chemical composition over a broad range of length scales.

1.1 Platforms

In principle, several different systems can serve as a basis for the mentioned platforms. As shown in Fig. 1, we will discuss in this contribution a variety of complementary 2D and quasi-3D architectures. SAMs of organothiols, disulfides or sulfides on gold [29, 59] and SAMs of organosilicon compounds on hydroxylated silicon surfaces [60–62] are probably among the best known model systems due to their ease of preparation and the high level of structural and chemical control. Vesicles (liposomes) [63] and substrate-supported lipid bilayers [64–67] are related well-established model systems for biological membranes that allow one to study membrane constituents in a controlled environment, and they can serve as a platform for biosensors based on naturally existing biomolecules present in a milieu that approximates a cell mem-

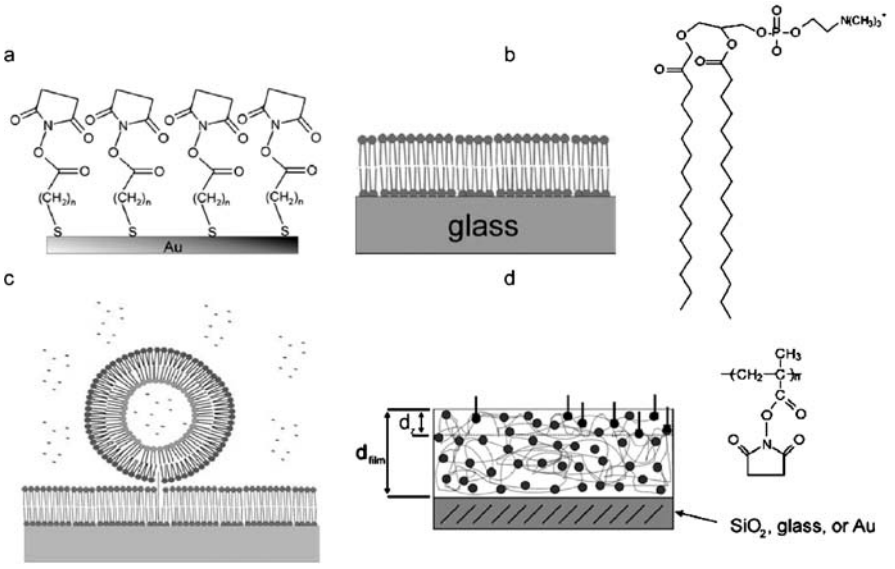

Fig. 1 Different platforms for biomolecule immobilization or biosensor surface modifications: **a** reactive ester-terminated SAM on gold; **b** substrate-supported lipid bilayer on glass (structure of 1.2-dimyristoyl-*sn*-glycero-3-phosphatidylcholine, DMPC); **c** substrate-immobilized lipid vesicle; **d** spin-coated thin film of a reactive homopolymer, such as poly(*N*)-hydroxysuccinimidyl methacrylate (PNHSMA; with tunable thickness d_{film}; the reactive groups are located in a region near the surface with depth d_z; the reactant molecules and reactive moieties in the film are schematically depicted as *bars* and *dots*, respectively)

brane [63]. Finally, substrate-supported (ultra)thin polymer films comprise an alternative platform for interfacing artificial (such as sensor) surfaces with biologically relevant media and systems [18, 68]. Even though structural control on a molecular level is less defined compared to SAMs, the tunable compositions of these systems, their unique polymer properties, such as swelling or presence of entropic forces under certain conditions, their robustness, as well as the facile control of layer thickness over a broad range make these systems attractive for certain applications. Polymers are also promising materials for overcoming the intrinsic limitations of 2D platforms. Such systems and approaches comprise hydrogels [16, 69–72] dendrimers [73–77], hyperbranched polymers [78], polymers prepared by chemical vapor deposition approaches [79], plasma polymers [80, 81], self-assembled polyelectrolyte mutilayers [82] and polymer brushes obtained by grafting-from approaches [83]. From this list we will only treat dendrimer systems in this review.

1.2 Patterning

Patterned surfaces are required for many application platforms [84]. As illustrated with examples from our and our collaborators' work (Fig. 2), SAMs on gold, lipid bilayers, and thin polymer films can be patterned using conventional photolithographic approaches [85], or unconventional approaches, such as soft lithography [86–89] and direct-write scanning probe lithography [90, 91]. Depending on the method utilized, pattern sizes of hundreds of micrometers to sub-100 nm are accessible in principle. The underlying principles of these approaches have been reviewed recently [86–91] and will be discussed, where necessary, in the corresponding sections of the review. Considering the broad range of length scales involved, it is clear that there is a need for a number of complementary approaches to patterned surface functionalization. In order to realize the stated objectives, knowledge of reactivity and its relation to structure of the assembly on the one hand and the analysis of local chemical composition on the other are also required.

1.3 Surface Chemistry in Ordered Systems

Besides the spatial control of surface modification (patterning), control over surface coverage (functional group densities) is a centrally important point. As in any organic chemical reaction, the functional groups involved, the medium and the reaction conditions (such as temperature) influence the reactivity. However, for surface-based reactions, additional factors must be taken into account [36, 37]. These include, among others, steric and anchimeric effects of the reactants, prevented or hindered access of the reactive species from the solution to the reaction centers, or interactions of neighbor-

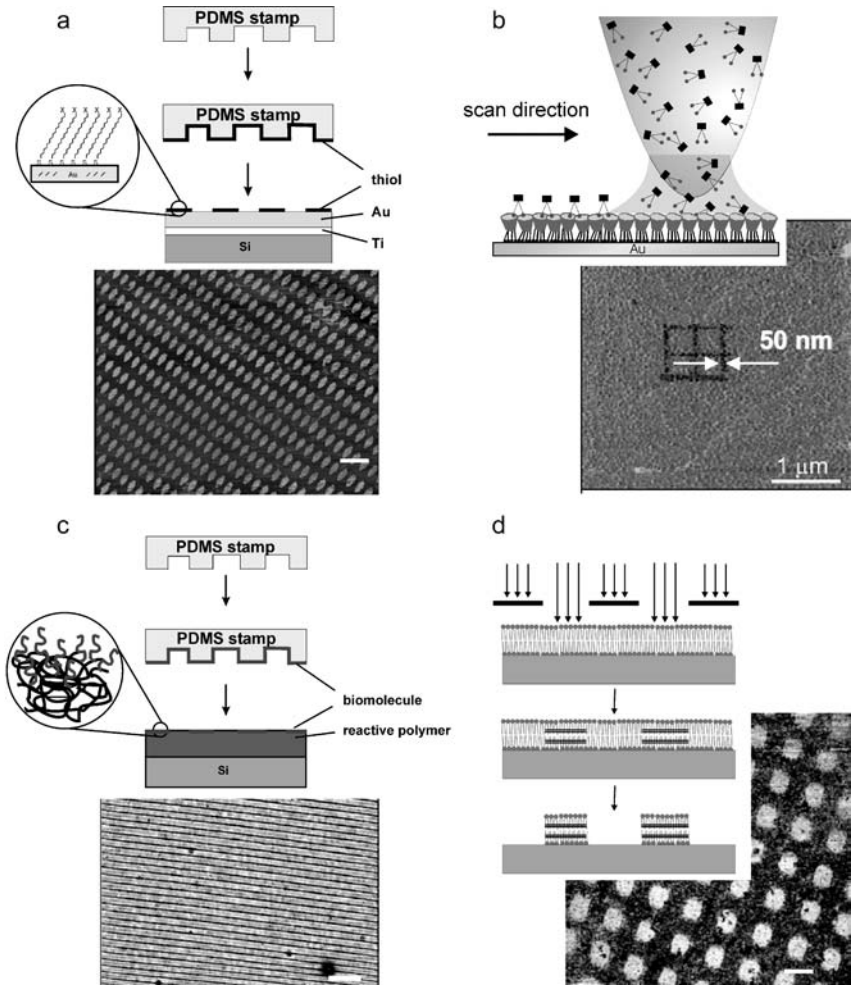

Fig. 2 Atomic force microscopy (AFM) friction images and schematic illustrations of the patterning processes of: **a** microcontact printed SAMs (mercaptoethanol dots in octadecanethiol matrix, scale bar 10 μm); **b** patterned molecular printboards fabricated by supramolecular dip-pen nanolithography (DPN) (reprinted with permission from [92]; Copyright 2004. Wiley VCH); **c** locally hydrolyzed *tert*-butyl acrylate-terminated polymer film on oxidized silicon (soft lithography; scale bar 3 μm) (Feng CL, Vancso GJ, Schönherr H, manuscript submitted to Langmuir); **d** photopatterned bilayer of diacetylene lipid (scale bar 10 μm). Reprinted in part with permission from [93], copyright (1999), American Chemical Society

ing functional groups with the reaction center or enrichment of reactants in disordered layers [94]. For monolayers, additional effects include interactions with the substrate, resulting in altered nucleophilicity and restricted reorientations of functional groups at the monolayer surface [95].

The local environments of the functional groups immobilized in densely packed SAMs, for instance, can also be significantly different from the typical situation in solution. Consequently, the reactivities of these groups may change, as judged from changes in local pK_A [96–100] for example. Similar pK_A changes observed on surface-treated polymers suggest that these phenomena are not limited to perfectly ordered assemblies, but may also be significant in more disordered systems [101, 102]. For optimized surface and interface chemistry in organized molecular assemblies and thin polymer films, it is therefore imperative to understand the underlying *structure–reactivity relationship*. This may include the effect of local order versus disorder and changes in reactivity that may accompany the transition from 2D to 3D architectures.

1.4 Challenges in Surface Characterization and Analysis

Since the effect of functional groups on the reactivities of neighboring functional groups may be highly localized (due to the range of the interaction forces) [103], and since heterogeneities of, say, polymer surfaces also span an enormously wide range, the necessary laterally resolved compositional analysis from micrometer to nanometer length scales is a second point of interest in this review. As reviewed recently [104, 105], there are different approaches that can be used to perform the compositional analysis of organic and polymeric surfaces; however, it was noted that both the experimental procedures and the theoretical background are still far from being fully developed. Laterally averaged chemical composition data, on the other hand, is readily available [106].

The images of the patterned systems shown in Fig. 2 are atomic force microscopy (AFM) friction force images, which display pronounced contrast between areas with different tribological properties [107]. The contrast is related to different surface properties, including surface free energy, and different mechanical responses, for example those arising from differences in molecular packing [108]. While the contrast appears to be sufficient for qualitative analysis, it is difficult to assess the surface coverage of a particular functional group or a particular molecular adsorbate in a quantitative manner based on the friction force contrast. Particularly in systems that are oriented anisotropically in-plane, friction forces on chemically homogeneous surfaces may depend on the relative orientation [109–113]. Complementary approaches comprise AFM force mapping [114–119], as well as various spectroscopies (infrared and Raman) [120], secondary ion mass spectrometry (SIMS) [121, 122], matrix-assisted laser desorption/ionization mass spectrometry (MALDI-MS) [123], X-ray photoelectron spectroscopy (XPS or ESCA) [124, 125], and near-field optical techniques [126] used for imaging.

This review will treat organic and macromolecular films and assemblies as (bio)reactive platforms starting from the analysis of structure–property and consequently structure–reactivity relationships in well-defined model sys-

tems (SAMs on Au, Fig. 3). The role of conformational order in determining the reactivity of NHS active esters in hydrolysis and aminolysis reactions will be discussed, as well as the analysis of reaction kinetics on the nanometer scale using inverted chemical force microscopy (iCFM). Then we will extend the SAM-based systems to quasi-3D systems using two complementary ap-

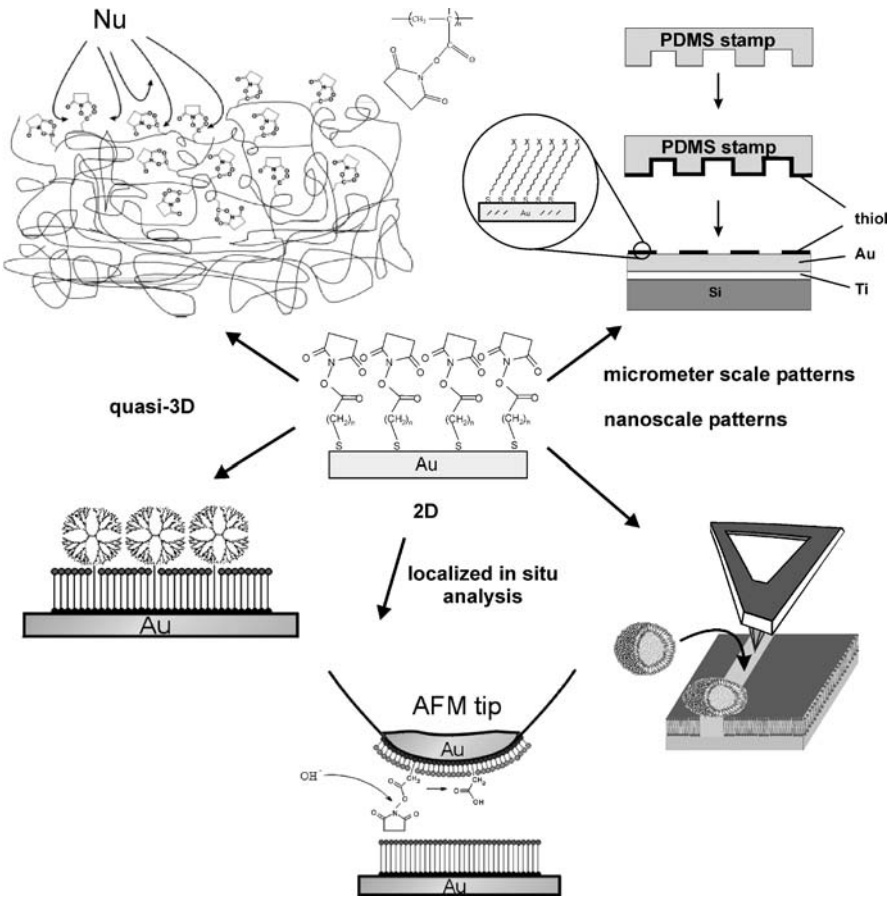

Fig. 3 Schematic of the different aspects of surface functionalization, patterning and analysis treated in this review. The topic is introduced and developed starting from the discussion of well-defined model systems (SAMs on Au). The determination of structure–reactivity relationships, and in particular the way conformational order affects the reactivity of NHS active esters will be discussed. Using iCFM, very localized information on surface reactions can be quantitatively measured in situ for SAM-based systems. The extension of the dimensionality to quasi-3D systems via the immobilization of dendrimers and the fabrication of thin reactive homopolymer films will be addressed, as well as micro- and nanopatterning approaches via soft and scanning probe lithography. Here we discuss SAM-based, as well as bilayer/vesicle-based systems

proaches, namely the fabrication of thin reactive homopolymer films and the immobilization of dendrimers. Finally, micro and nanopatterning via soft and scanning probe lithography will be discussed for SAM-based, bilayer and vesicle-based systems.

2
Ultrathin Organic and Macromolecular Films and Assemblies as (Bio)reactive Platforms

The surface reactivities of ultrathin organic and macromolecular films and assemblies are of central importance to the targeted immobilization reactions of biomolecules. Compared to reactions that occur rapidly in solution, steric effects and locally altered environments may adversely affect reactivity in substrate-supported architectures [36, 37]. Hence the relationship of layer structure to reactivity, highly localized in situ analysis of surface chemical reaction kinetics, and the maximization of surface coverage (molecular loading) by extending the dimensionality of the reactive platform from 2D to quasi-3D will be elaborated on in the following sections.

2.1
Structure-Reactivity Relationships: Model Studies

As mentioned in the *Introduction*, it has been shown that chemical reactivity in ordered ultrathin organic films, such as Langmuir monolayers at the air–water interface [58], or SAMs on solid supports [36, 37], can be distinctly different from reactions carried out in solution. Since the functional groups or molecules involved in these reactions are immobilized at interfaces or on surfaces, these differences can be attributed to "confinement effects" [127]. As shown below, this reduction of reactivity is also present in substrate-supported thin polymer films, albeit to a different extent [128]. The discussion is structured by increasing the level of complexity, starting out with very well defined SAMs on gold.

2.1.1
Hydrolysis of NHS Ester SAMs

We focus initially on the relationship of SAM structure to reactivity for SAMs of activated NHS esters, which are versatile reactive functional groups utilized for the covalent coupling of biologically relevant molecules to surfaces [129–133]. It is well established that the conformational order of SAMs is a function of adsorbate chain length [134]. Since structure (as a result of confinement for example), local order and packing of functional groups appear to be related (see above), differences in conformational order likely result in different

reactivities. To this end the conformational order and the kinetics of the base-catalyzed hydrolysis of SAMs of *n*,*n*′-dithiobis(*N*-hydroxysuccinimidyl *n*-alkanoate) (NHS – C*n*, *n* = 2, 10, 15) were elucidated by grazing angle reflection (GIR) FTIR spectroscopy (Fig. 4) [127].

The FTIR spectra of SAMs of NHS – C2, NHS – C10, and NHS – C15 are shown in Fig. 5. The most prominent bands are the asymmetric C – H stretching vibration, ν_{as} (CH_2), at ~2920 cm^{-1}, the symmetric C – H stretching vibration, ν_s (CH_2), at ~2850 cm^{-1}, and the C = O stretching vibration, ν (C = O), at ~1748 cm^{-1}. For the complete band assignments and listing of peak positions [131, 132, 135], as well as other complementary characterization data, we refer to [127].

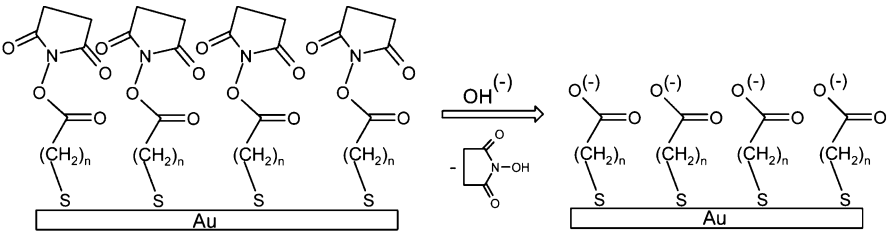

Fig. 4 Structure of NHS ester-functionalized SAM on gold (*n* = 2, 10, 15) and hydrolysis reaction in aqueous NaOH

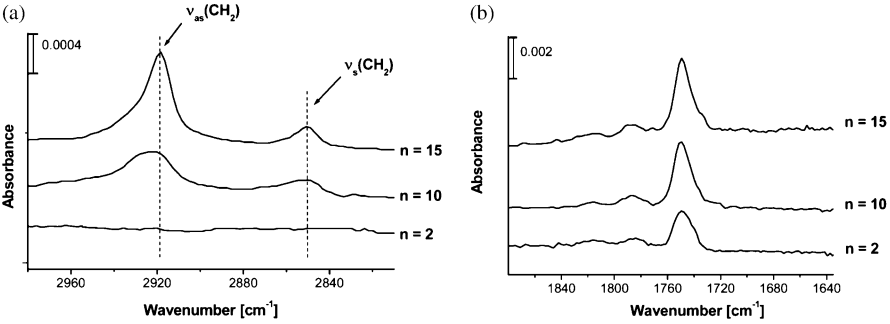

Fig. 5 **a** High-energy region of GIR-FTIR spectra of SAMs of NHS – C_n with *n* = 2, 10, and 15 on gold showing the C – H stretching vibrations. **b** Low-energy region of GIR-FTIR spectra of SAMs of NHS – C_n with *n* = 2, 10, and 15 on gold showing the succinimidyl and ester carbonyl C = O stretching vibrations. The spectra have been normalized to the absorbance of the C – D stretching vibrations of d_{33}-hexadecanethiol on gold used to record the background spectra. The integrated absorbance of the succinimidyl C = O stretching vibrations in the normalized spectra shown in Fig. 5b suggests a lower coverage for decreasing chain length of the disulfide, provided that the mean orientation of the transition dipole moments is similar. Furthermore, the peak width at half-maximum increases monotonically for decreasing chain length, which is indicative of a more disordered arrangement of the NHS ester end groups in the short chain disulfides. (Reprinted with permission from [127], copyright (2003), American Chemical Society)

The peak positions of the ν_s (CH_2) and ν_{as} (CH_2) modes for the NHS – C15 monolayers (2850 cm^{-1}, 2918 cm^{-1}) are shifted to lower frequencies compared the NHS – C10 monolayers (2852 cm^{-1}, 2922 cm^{-1}). These modes are unrecognizable in SAMs of NHS – C2, probably due to a broadening of the bands (the broadening of bands attributed to C – H stretching vibrations is obvious even for SAMs of NHS – C10). The band positions are consistent with *near-crystalline packing* of NHS – C15 in SAMs, while SAMs of NHS – C10 and NHS – C2 resemble *more disordered, liquid-like* SAMs [134]. Contact angle (CA) measurements with water as a probe liquid are fully consistent with this interpretation. The hysteresis decreases from 21° and 16° for SAMs of NHS – C2 and NHS – C10, respectively, to 10° for NHS – C15 [127].

The impact of the pronounced conformational differences of these SAMs on their reactivities was assessed by GIR-FTIR and CA measurements for the well known ester hydrolysis in alkaline medium. These measurements were performed in an ex situ mode for samples immersed in the appropriate solutions for variable periods of time followed by extensive rinsing. The kinetics was determined by measuring the decrease in the integrated intensity of the succinimidyl carbonyl band, as shown in Fig. 6a for a NHS – C10 SAM hydrolyzed in 1.00×10^{-2} M NaOH. The strong band at 1748 cm^{-1} decreases in absorbance as the reaction progresses. The extent of the base-catalyzed reaction x can be expressed as a function of hydrolysis time

$$x = \frac{A_0 - A_t}{A_0 - A_\infty}, \tag{1}$$

where A_0 is the integrated absorbance of the succinimide ester carbonyl band at time zero, at time t, and A_∞ is at infinitive time, respectively.

$$\cos\theta_{exp} = \chi_{NHS} \cos\theta_{NHS} + \chi_{COOH} \cos\theta_{COOH}, \tag{2}$$

where χ_{NHS} and χ_{COOH} are the surface coverages of the two components and $\theta_{NHS} = 59 \pm 2°$ and $\theta_{COOH} = 0°$ are the contact angles of the two pure SAMs.

Similarly, CA measurements were used (in conjunction with the Cassie equation) [136] to estimate the corresponding surface coverages. For conversions of < 50%, FTIR and CA data are in quantitative agreement [128].

As shown in Fig. 6b, the reaction kinetics for identical reaction conditions (1.00×10^{-2} M NaOH at 30 °C) differ significantly for NHS ester SAMs with different chain lengths. While NHS – C2 and NHS – C10 display pseudo first order kinetics with different rate constants (Table 1), NHS – C15 shows the presence of an induction period (see inset in Fig. 6b).

Compared to the hydrolysis reactions of NHS ester model compounds in solution, [136] we observe a decrease in the apparent rate constants by 2–3 orders of magnitude for NHS – C2 and NHS – C10. More strikingly, the reaction of the NHS esters in the highly ordered SAM NHS – C15 shows a different overall kinetic profile. Instead of the expected pseudo first order (exponential) kinetics, sigmoid kinetics with a pronounced induction period are found.

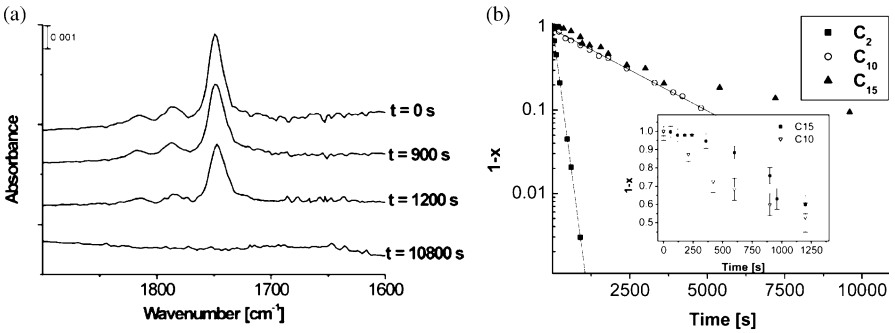

Fig. 6 **a** GIR-FTIR spectra for NHS – C10 hydrolyzed for different times in 1.00×10^{-2} M NaOH at 30 °C; (Reprinted with permission from [127]; Copyright (2003) American Chemical Society). **b** linearized kinetics plot of hydrolysis for NHS – C*n* for $n = 2$, 10, and 15 (1.00×10^{-2} M NaOH at 30 °C), *inset*: comparison of early stages of hydrolysis of C10 and C15 systems

Table 1 Rate constants and half-lives of the reactions obtained for the NHS – C_n esters

	k''_{FTIR} [M^{-1} s^{-1}]	k''_{CA} [M^{-1} s^{-1}]	$\tau_{1/2}$ (FTIR) [s]	$\tau_{1/2}$ (CA) [s]
$n = 2$	$(61 \pm 11) \times 10^{-2}$	$(56 \pm 23) \times 10^{-2}$	117 ± 5 [a]	124 ± 5 [a]
$n = 10$	$(4.5 \pm 0.4) \times 10^{-2}$	$(4.5 \pm 2.3) \times 10^{-2}$	1540 ± 10 [a]	1500 ± 10 [a]
$n = 15$	–	–	1700 ± 20 [b]	1700 ± 20 [b]
bulk [c]	8700×10^{-2} [c]	8700×10^{-2} [c]	0.8 [c]	0.8 [c]

[a] Calculated as $\tau_{1/2} = \ln 2/k'$ for a base concentration of 1.00×10^{-2} M
[b] Measured for a base concentration of 1.00×10^{-2} M
[c] Data obtained/recalculated from [137]

This change in the rate law with increasing chain length can be attributed to tighter packing of the ester groups as a result of the increasing conformational order. Consequently, access to the hydroxide ions is much more hindered compared to reactions of short chain SAMs [29]. The observed behavior is consistent with a reaction that starts at defect sites and accelerates as more reactive site become accessible as a consequence of the initially reacted ester groups. However, the nature of the induction period is difficult to unravel by FTIR and CA measurements, owing to the lack of spatially resolved information. The surface chemical composition and wettability are assessed as a mean value over almost macroscopic distances (on the order of 10^{12}–10^{14} molecules are probed). Before we elucidate how AFM approaches can be utilized to analyze surface reactions at the relevant length scale in order to help unravel the nature of, say, the previously mentioned induction periods, a second class of reactions of NHS esters are discussed.

2.1.2
Aminolysis of NHS Ester SAMs

The relevance of NHS esters stems from their role as reactive groups that are susceptible to nucleophilic attack, for example from primary amino group-containing molecules (also in aqueous medium). NHS esters are hence frequently utilized to immobilize biomolecules on surfaces via covalent attachment reactions of primary amino groups. Examples include amino end-functionalized DNA, proteins or antibodies [129–133].

As a simple model reaction for such immobilizations, we investigated the reaction of NHS – C10 SAMs and *n*-butyl amine in aqueous medium [138, 139]. The coupling reaction was followed analogously to the hydrolysis discussed above by ex situ GIR-FTIR and CA measurements. The corresponding FTIR spectra, as well as the reaction kinetics assessed by both methods, are shown in Fig. 7.

During the reaction of SAMs of NHS – C10 with *n*-butylamine, the appearance of the CH_3 asymmetric in-plane CH stretching mode ($\nu_a(CH_3, ip)$, 2966 cm^{-1}), the CH_3 symmetric CH stretching mode ($\nu_a(CH_3, FR)$, 2879 cm^{-1}), and the amide I (1650 cm^{-1}) and amide II (1550 cm^{-1}) bands are diagnostic of the amide groups formed during the reaction [140]. The kinetics can be determined in a similar way to the hydrolysis by analyzing the integrated absorbance of pronounced bands in the FTIR spectra ($\nu_a(CH_3, ip)$ and succinimide C = O) and by analyzing the CA data using the Cassie equation. The half-lives of the aminolysis reaction, as determined using both methods, are in good agreement ($\tau_{1/2}(FTIR) = 2685 \pm 40$; $\tau_{1/2}(CA) = 2800 \pm 40$).

The deviation of the kinetics from the simple pseudo first order kinetics observed for the hydrolysis is certainly related to the differences in size and nucleophilicity of the attacking nucleophile. Similar to the induction period observed for the hydrolysis of NHS esters in SAMs of NHS – C15 on gold,

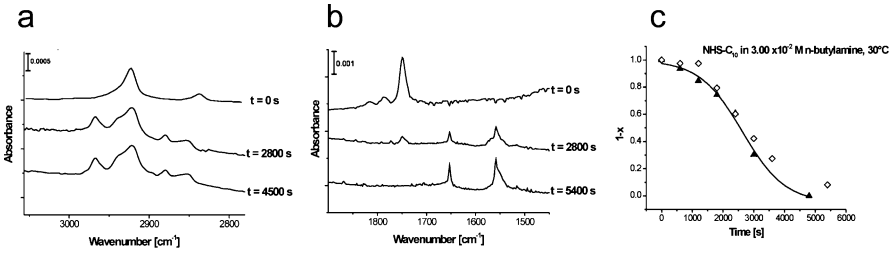

Fig. 7 **a** High-energy region and **b** low-energy region of GIR-FTIR spectra of SAMs of NHS – C10 on gold after different reaction times with 3.00×10^{-2} M aqueous *n*-butylamine at 30 °C (Reprinted from [139], copyright (2004), with permission from Elsevier). **c** Reaction kinetics obtained from the analysis of the GIR-FTIR and CA data (*right*). (Reprinted from [138], copyright (2004), with permission from Elsevier)

a laterally inhomogeneous reaction, which starts at initiation sites, would offer a plausible explanation. Based on the mean domain size of ~ 5 nm reported for SAMs on gold [141], one may expect that the relevant length scale is $< 50-100$ nm. However, without high-resolution compositional information acquired with this level of lateral resolution, such an interpretation remains speculative. Hence, the development of new approaches to characterizing local chemical surface compositions is needed.

2.1.3 Analysis of Reaction Kinetics on the Nanometer Scale: iCFM on NHS – C10 SAMs

The apparent limitations of spatially resolved ex situ analysis and interpretation of the reaction kinetics of surface reactions on soft (organic and polymeric) surfaces, using methods such as GIR-FTIR, CA and other established methods (including XPS and SIMS), was highlighted in the previous sections. Methods for performing in situ analysis of the reaction kinetics of wet chemical surface reactions with sufficiently high resolution are largely unknown [104, 105]. One exception is the family of scanning probe microscopies. So-called chemical force microscopy (CFM) [142] has demonstrated its potential for discriminating areas with different chemical compositions down to sub-50 nm length scales [143]. Using chemically functionalized tips, pull-off forces measured in force–displacement measurements contain information about the surface and interfacial free energies of the contacting surfaces and hence constitute a way to estimate surface coverages in simple reactions with high lateral resolution.

To circumvent the problems of instrumental drift during intrinsically slow in situ force mapping of wet chemical reactions on surfaces (a 64×64 pixel^2 map is typically acquired in several minutes), we introduced an AFM-based technique called inverted CFM [29]. In this approach, the reactants are immobilized on the AFM tip and *not* on the flat sample surface (Fig. 8). The flat surface consists of an inert SAM on Au(111). To follow the kinetics of the reactions of the tip-immobilized functional groups, the variation in pull-off forces between the tip coated with the reactant and the inert surface is monitored as a function of time in situ in the reaction medium. The contact area of the tip at the pull-off in such experiments using nonreactive SAMs deposited on atomically flat Au(111) (as inert samples) varies (depending on the surface free energies) between approximately 10 and 100 effectively interacting molecular pairs [138, 139]. However, as the surface characteristics of the inert substrate do *not* vary as a function of position, the pull-off force values only contain compositional information about those reactant groups on the tip that reside inside the tip–sample contact area. As shown below, this approach can provide some information that is lacking about surface reactions that display an induction period.

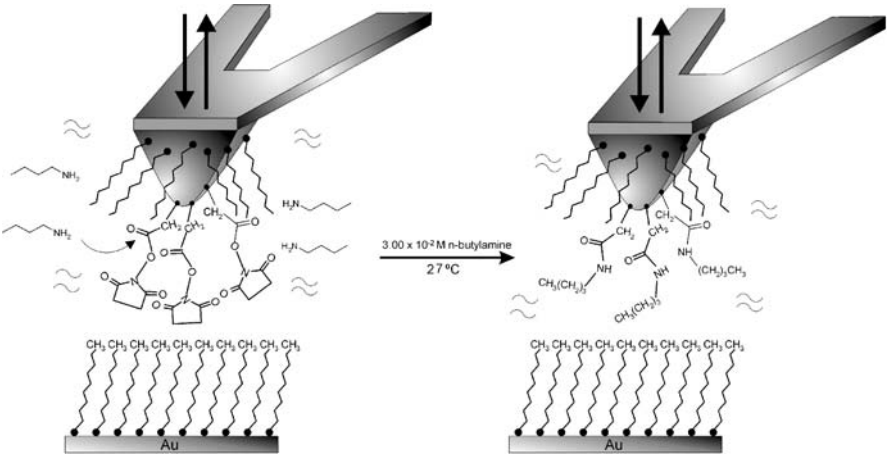

Fig. 8 Schematic drawing of "inverted" chemical force microscopy for the reaction between NHS-esters and *n*-butylamine in aqueous medium. In iCFM the pull-off forces between an AFM tip covered with a SAM of NHS – C10 and an inert octadecanethiol SAM are measured in situ during the conversion of the reactive groups attached to the tip. The interaction between tip and inert surface varies systematically with the extent of the reaction and hence it allows one to quantitatively investigate the reaction kinetics. (Reprinted from reference [139], copyright (2004), with permission from Elsevier)

To obtain a better understanding of the sigmoid kinetics observed for hydrolysis and aminolysis reactions, as discussed in the previous sections, these reactions were investigated on the nanometer scale by iCFM. In these experiments the force required to pull gold-coated AFM tips functionalized with SAMs of NHS – C10 away from contact with an inert octadecanethiol (ODT) SAM on flat Au(111) was monitored in real-time during reaction in aqueous NaOH and *n*-butylamine for hydrolysis and aminolysis, respectively.

As shown in Fig. 9, the pull-off forces (each data point represents the mean value of 200 individual pull-off events) were found to *decrease* for the hydrolysis, while the forces *increased* for the aminolysis. The changes in pull-off force were directly related to changes in surface composition of the contact area at pull-off.

The pull-off force $F_{\text{pull-off}}$ can be expressed as function of tip radius R and work of adhesion (surface energy per unit area) W_{12} as

$$F_{\text{pull-off}} = -3/2\pi R W_{12} \tag{3}$$

W_{12} is a function of the surface free energies of the tip (γ_1), the sample γ_2, and the corresponding interfacial free energy γ_{12} (Eq. 4). If the experiment is carried out in a medium, the γ_i refer to the surface free energy for the surface i

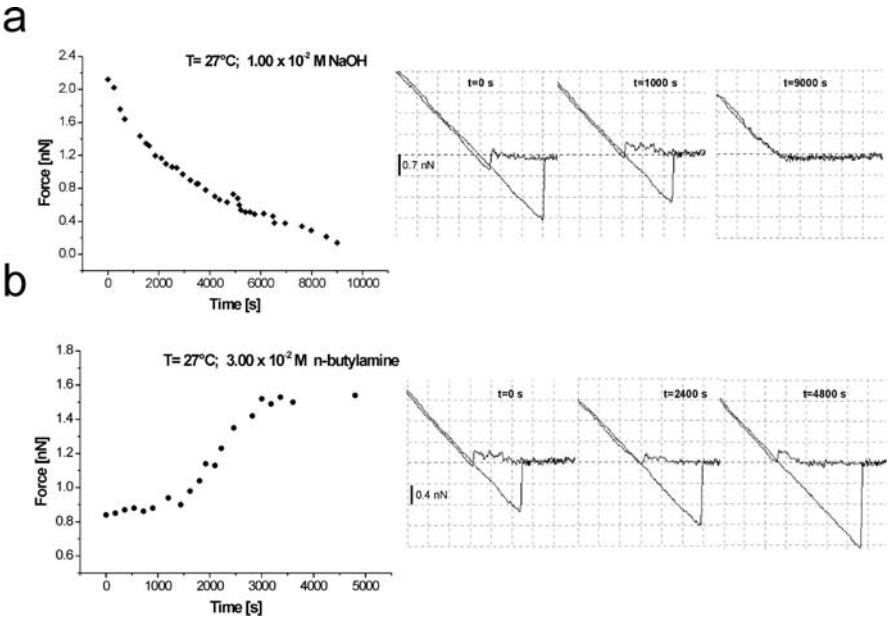

Fig. 9 Plot of pull-off forces as function of reaction time during hydrolysis (**a**) and aminolysis (**b**) of NHS – C10 determined by iCFM. Each data point corresponds to the mean pull-off value of 200 individual pull-off events. Representative force–displacement curves are shown as insets. ($F \propto$ extent of reaction) (Reprinted from [138], copyright (2004), with permission from Elsevier)

in contact with the corresponding medium.

$$W_{12} = \gamma_1 + \gamma_2 - \gamma_{12} \tag{4}$$

The conversion x of ester groups to carboxyl and amide groups was calculated from:

$$x = \frac{F_0 - F_t}{F_0 - F_\infty} \tag{5}$$

where F_0, F_t and F_∞ denote the measured average pull-off forces at $t = 0$, $t = t$, and $t = \infty$, respectively. This equation assumes that the forces change linearly with the work of adhesion.

Each curve represents the kinetics of the reaction occurring *exclusively* in the contact area of an *individual* AFM tip modified with a SAM of NHS – C10. The observed trends are fully consistent with solvent exclusion effects [144]. Increasing conversion leads to a progressively more solvated carboxylate surface in the case of the hydrolysis, while for the aminolysis an increasingly less solvated, hydrophobic surface is obtained.

For the hydrolysis each experiment displayed an exponential decrease in the pull-off force, which can be linearly transformed to surface coverage via

Eq. 3. Thus, the data is consistent with pseudo first order kinetics for the hydrolysis; furthermore, the absence of any induction period points to a spatially homogeneous hydrolysis reaction on the mentioned length scale. The corresponding rate constants are summarized in Table 2.

By contrast, widely different individual force (reaction) profiles were observed for the aminolysis reaction. Most of the profiles showed an induction period, after which the pull-off forces increased and finally leveled off. A number of representative individual traces are shown in Fig. 10a. Figure 10b shows a histogram of the induction periods observed for the aminolysis, as well as a plot of the experimentally determined induction period vs the number of effectively interacting molecular pairs (evaluated by the JKR [145] and the Poisson [146] approaches, respectively).

The experimental data indicate that the aminolysis reaction may spread from initiation or defect sites that are initially accessible for nucleophilic attack. At a very early stage, the reaction proceeds very slowly, as generally seen by FTIR spectroscopy (Fig. 7), because larger numbers of accessible reactive groups in the monolayer must first be generated as a consequence of the initial hydrolysis reaction. As more accessible reactive groups form, the reaction accelerates. The observation of a broad range of induction periods is fully consistent with this model. The reaction can be detected at or just after the start of the experiment (Fig. 10: $t_{ind} \leq 200$ s), if initiation or defect sites are present in or are close to the small tip-sample contact area. For initiation or defect sites outside of this contact area there are initially no changes in pull-off force. The highly localized observation of the reaction only starts after the reaction has proceeded to the tip–substrate contact area (Fig. 10: $t_{ind} > 800$ s).

Consistent with this interpretation, the averaged force versus time data reproduces the sigmoid conversion observed on the macroscale (Fig. 7c), as seen by the excellent agreement of the mean half-life of the reaction in 3.00×10^{-2} M aqueous *n*-butylamine of 2600 ± 240 s and the half-life of

Table 2 Kinetic parameters for reactions of SAMs of NHS – C10

reaction	k'' [M^{-1} s^{-1}]	$\tau_{1/2}$ [s]
hydrolysis (FTIR) at $T = 30$ °C	$(4.5 \pm 0.4) \times 10^{-2}$	1540 ± 10 [a]
hydrolysis (CA) at $T = 30$ °C	$(4.5 \pm 2.3) \times 10^{-2}$	1500 ± 10 [a]
hydrolysis (iCFM) at $T = 27$ °C	$(3.0 \pm 0.2) \times 10^{-2}$	2310 ± 20 [a]
aminolysis (FTIR) at $T = 30$ °C	–	2685 ± 40 [b]
aminolysis (CA) at $T = 30$ °C	–	2800 ± 40 [b]
aminolysis (iCFM) at $T = 27$ °C	–	2600 ± 240 [b]

[a] Calculated as $\tau_{1/2} = ln2/k'$ for a base concentration of 1.00×10^{-2} M.
[b] Measured for 3.00×10^{-2} M aqueous *n*-butylamine.

2685 ± 40 s estimated from the FTIR data (Table 2) for the aminolysis. From the regression analysis in Fig. 10b we can estimate that the average number of effectively interacting molecular pairs, for which the induction period vanishes, corresponds to 85 ± 4 pairs (Poisson) and 77 ± 3 pairs (JKR) (area $\sim 20\,\text{nm}^2$). Based on the interpretation that the reaction starts at defect or initiation sites, this value corresponds to 5×10^{12} defects/cm^2 and an approximate mean distance between neighboring defects of ≥ 5 nm. As there are several thousand pinholes/cm^2 in etch-resistant SAMs of, say, ODT on gold [147], the initiation sites are unlikely to be pinholes, but may be defects in optimal head group packing.

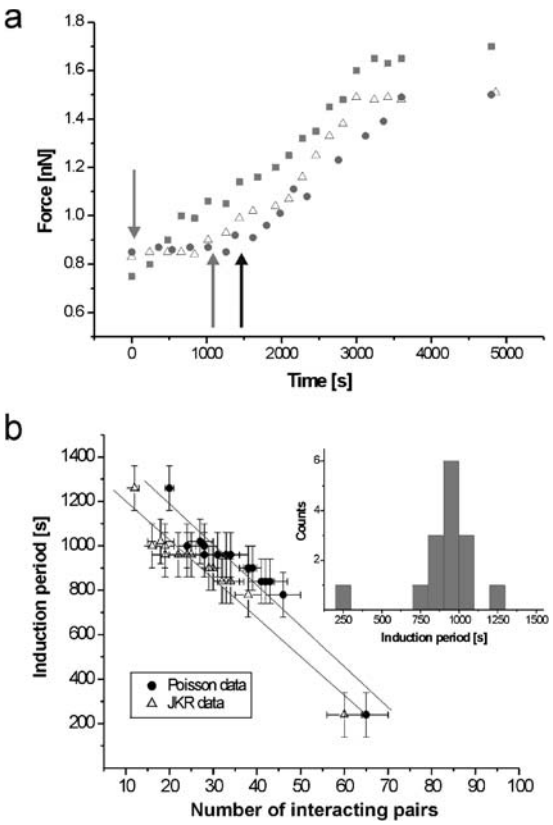

Fig. 10 **a** Three individual aminolysis reactions followed by iCFM force measurements. The *arrows* indicate three widely different induction periods of ~ 0 s, ~ 1000 s, and ~ 1450 s; **b** Plot of induction period vs number of interacting pairs estimated using both the JKR theory and the Poisson method (*inset*: histogram of induction periods as measured by iCFM during aminolysis of NHS – C10). (Reprinted from [138], copyright (2004), with permission from Elsevier)

In conjunction with the results of the previous sections, it appears that a high degree of conformational order and tight packing in, say, monolayer systems, is detrimental for realizing highly reactive platforms for the immobilization of (bio)molecules with high molecular loading. Direct molecular level evidence by iCFM points to the presence of laterally heterogeneous reactions for highly ordered systems. The difference between the two types of model reactions also underlines the importance of the size and character of the nucleophile for obtaining reactive systems with simple and predictable kinetics. Further insight into the relationship of structural order to reactivity was sought in comparative studies of the temperature dependence of model reactions in SAMs and related spin-coated polymer thin films.

2.1.4
Determination of Activation Energies for NHS – C10 Ester SAMs versus NHS Homopolymer Thin Films

Analysis of the temperature dependence of surface chemical reactions will provide a more detailed insight into the underlying factors that may hamper the corresponding surface reactions. Using the CA approaches introduced above, the surface compositions of SAMs of NHS – C10 and thin films of poly(*N*-hydroxysuccinimidyl methacrylate) (PNHSMA) on oxidized silicon (Fig. 11) were determined after reaction in alkaline media at different temperatures [128]. FTIR spectroscopy provides complementary information, but owing to their limited surface sensitivity, spectroscopic methods are inferior to CA measurements [148].

The kinetic data show that the NHS ester groups in PNHSMA are hydrolyzed in a reaction that can be described as a pseudo first order reaction for all temperatures with an apparent (second order) rate constant that is ~ 5 times faster than for the SAM of NHS – C10 on gold. In Fig. 11, the corresponding data has been plotted according to the linearized form of the Arrhenius equation (Eq. 6).

$$\ln k'' = \ln A - \frac{E_a}{RT}, \tag{6}$$

where k'' is the second order rate constant, A the pre-exponential (Arrhenius) factor, E_a the activation energy, R is the gas constant, and T is the absolute temperature.

The activation energy and the Arrhenius pre-factor can be obtained from the slope and the intercept. The latter factor can yield the parameters of the transition state, such as the entropy of the transition state (Eq. 7).

$$\Delta S^{\ddagger} = R(\ln \frac{A}{T} - \ln \frac{k_b}{h} - 1), \tag{7}$$

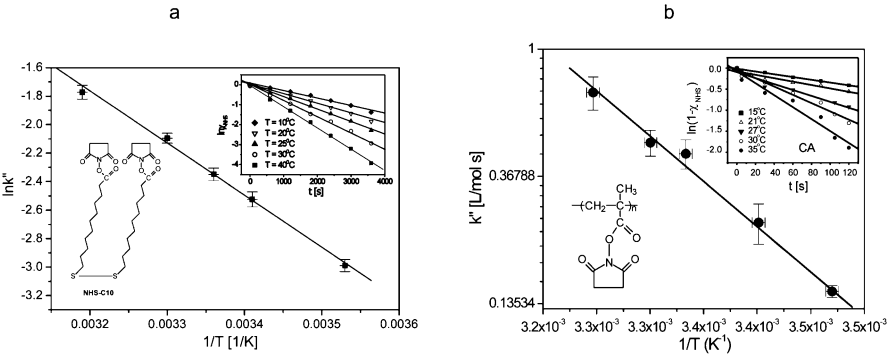

Fig. 11 Arrhenius plots for **a** NHS – C10 SAM and **b** PNHSMA. The *solid lines* correspond to linear least squares fits of the data (*insets*: linearized kinetics for different temperatures for SAM and PNHSMA evaluated based on CA measurements; linearization according to pseudo first order kinetics of the NHS ester surface coverage data calculated from the corresponding CA data using the Cassie equation). (Adapted with permission from [128], copyright (2003), American Chemical Society)

Table 3 Activation energies and estimated parameters characterizing the transition state of the aqueous NaOH

Sample	E_a [kJ/mol]	$\Delta S^{\ddagger}$ (298 K) [J/mol K]
NHS – C10	30 ± 1	– 170
PNHSMA	61 ± 2	– 60

where $\Delta S^{\ddagger}$ is the activation entropy, k_b is the Boltzmann constant, and h is Planck's constant.

The activation energies (Table 3) show a different trend than the rate constants. Compared to SAMs of NHS – C10, the activation energies are significantly higher for the surface reaction of PNHSMA. These observations can be attributed to an increase in mobility and flexibility in the polymer films compared to the SAMs. For the surface region of PNHSMA, the activation entropy is far less negative than for the SAMs, which means that the hydrolysis of NHS – C10 is characterized by a tighter and sterically more demanding transition state.

These data are most consistent with differences in structure between NHS – C10 and PNHSMA – a tightly packed SAM with slight conformational disorder versus an amorphous polymer film in which the NHS ester groups cannot be tightly packed (Fig. 12). In the former case fewer degrees of freedom are available compared to the polymer films. These differences in structure appear to be intimately linked to the kinetic and thermodynamic

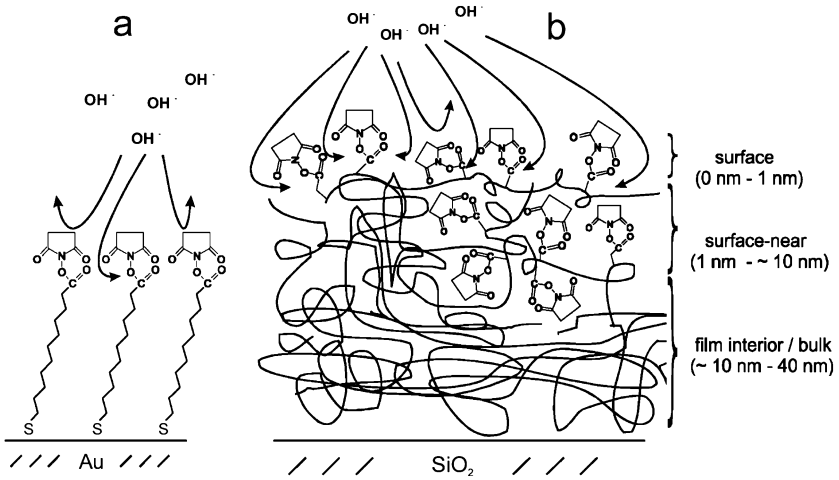

Fig. 12 Schematic of base-catalyzed hydrolysis reaction in **a** SAMs of NHS – C10 and **b** ultrathin films of PNHSMA on oxidized silicon together with the definitions of surface and surface-near regions of the polymer film. The approximate depths in this tentative model were assigned based on the information depths of the techniques (CA: 1 nm [148], IR: the entire film, in other words 40 nm), the fact that only 25% of the NHS ester groups can be hydrolyzed, and that the reaction can be expected to start at the film-solution interface and to proceed homogeneously into the amorphous film. (Reprinted with permission from [128], copyright (2003), American Chemical Society)

parameters of the reactions and the corresponding transition states, respectively. Hence we can conclude that careful design of the organic thin film structure will allow one to control the reactivity in wet chemical reactions, including the immobilization of, say, DNA.

Together with very recent results that show an increase in surface coverage of, for instance, immobilized amino-group-terminated poly(ethylene glycol) (Feng CL, Vancso GJ, Schönherr H, unpublished work) by a factor of 3–4, the much less restricted reactivity of simple reactive homopolymer films is an attractive feature for applications that require robust reactive coatings with high molecular loading. These systems are amenable to the patterning procedures that will be discussed in the following sections. However, the organized assemblies discussed offer the advantage of a higher degree of definition, which facilitates their quantitative characterization and thus the derivation of general guidelines based on these model studies.

2.2
Micro- and Nanofabrication of High Loading (Bio)reactive Surfaces

The drawback of reduced reactivity due to steric crowding found in highly organized monolayer architectures and the inherently limited loading can be

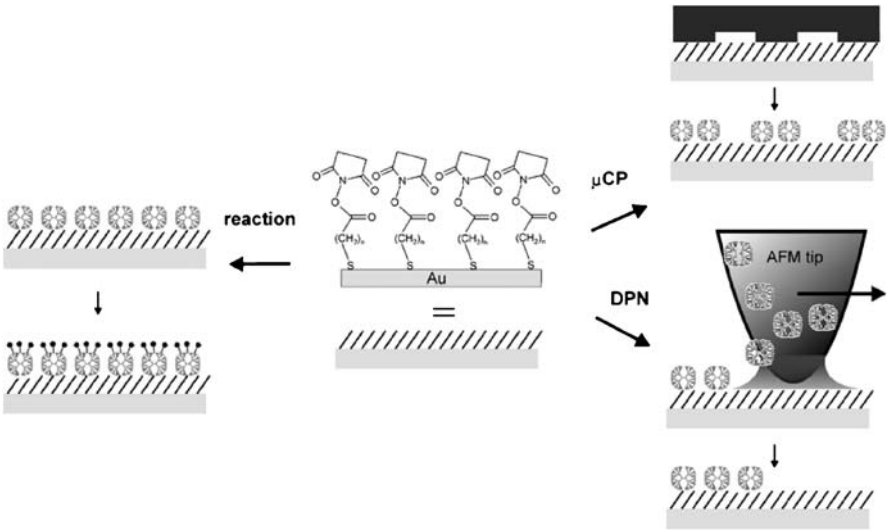

Fig. 13 Schematic of immobilization of amino-terminated PAMAM dendrimers to NHS reactive ester SAMs on gold via covalent bond formation; reaction from solution provides homogeneously covered layers that can be labeled in order to determine the number of retained primary amino groups of the dendrimers. Micro and nanometer-scale patterning is possible via μCP and DPN

circumvented by utilizing well-defined macromolecular thin films. The extension of 2D architectures to the third dimension is an attractive way to increase the loading of (bio)molecules on reactive surfaces and to reduce the effects of steric crowding at the same time. The latter effects have only be considered in the context of actual immobilization chemistry so far. However, it is clear that any biosensor or biochip must present the immobilized species in its active form, such that the interactions to be studied (DNA hybridization, antibody–antigen interactions, and so on) are not hindered by spatial constraints due to tight packing on the sensor or chip surface. For example, the optimized surface coverage for 2D architectures (SAMs) for biotin–streptavidin interactions has been reported to be as low as $\chi = 0.1$ [149].

Recently, reactive platforms based on well-defined macromolecules, such as dendrimers [75, 150], have been introduced as reactive layers that expose chemically accessible functional groups in high densities. These approaches can be extended to micro- and nanoscale patterns by means of microcontact printing (μCP) [86–89] and scanning probe lithography (AFM tip-assisted deposition, also called "dip-pen nanolithography", DPN) [90], as reviewed below (Fig. 13).

2.2.1
Covalent Coupling of Dendrimers to NHS Ester SAMs

To obtain robust reactive ultrathin films with high molecular loadings, in which steric interactions are minimized, covalent attachment of dendrimers to reactive SAMs has been investigated [77]. As shown schematically in Fig. 13, amino group-terminated PAMAM dendrimers can be immobilized on reactive NHS – C10 SAMs by coupling from methanolic solution. The process can be conveniently followed by ex situ FTIR, among other techniques [77]. Upon immobilization, the typical C = O vibration of the NHS ester SAM gradually disappears at the expense of the pronounced amide I and amide II vibrations of the PAMAM dendrimers (Fig. 14a). Since the dendrimers contain a significant number of internal amide bonds that contribute to these latter peaks, complementary experiments with polypropylene imine dendrimers with amine termination (DAB) dendrimers have been carried out.

The dendrimer immobilization can be described by a Langmuir isotherm (Fig. 14b). Complementary XPS analyses in conjunction with labeling of the primary amino groups with trifluoroacetic acid anhydride showed that 28% of all the peripheral primary amino groups are chemically accessible (corresponding to an area requirement for each accessible amino group of $\sim 8.9 \times 10^{-19}$ m^2).

The immobilized G4 PAMAM dendrimers can be directly visualized using intermittent contact (tapping) mode AFM. As shown in Fig. 15, the dendrimers attached to NHS – C10 SAMs appear as globular features with heights

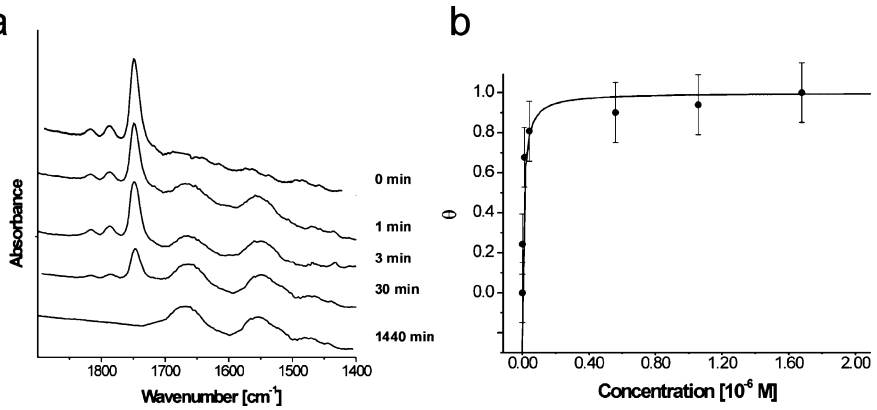

Fig. 14 **a** GIR-FTIR spectra of NHS – C10 SAM after reaction with G4 PAMAM dendrimers for various times (4.5×10^{-6} M methanolic solution of PAMAM G4). **b** Adsorption isotherm of PAMAM G4 on NHS – C10. The *solid line* corresponds to the fit of the Langmuir isotherm (reprinted with permission from [77], copyright (2004), American Chemical Society)

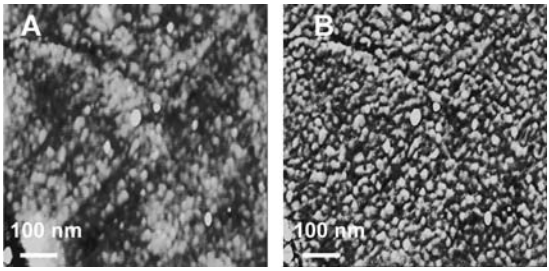

Fig. 15 **a** Tapping mode AFM height image (acquired in air, *z*-scale = 5.0 nm) and **b** phase image of NHS – C10 SAM fully covered with PAMAM G4. The triangular terraces of Au(111) are clearly recognizable in the height image (*left*), indicating that a layer of homogeneous thickness has been deposited. (Reprinted with permission from [77], copyright (2004). American Chemical Society)

of ~ 2 nm and (convoluted) widths of between 10 and 15 nm. These values are consistent with the interpretation that the features are indeed individual dendrimers, considering the theoretical diameter (4.5 nm) [151] and tip convolution effects. The AFM data shows that highly defined layers are formed, because the triangular terraces of the underlying Au(111) substrate can be still recognized. While these layers comply with the requirements identified in the previous sections, patterning appears to be a necessary condition for many biosensor and related applications.

2.2.2
Micropatterning of Dendrimers by Microcontact Printing

Patterning of SAMs can be performed by a multitude of techniques, as reviewed recently [152, 153]. Apart from photolithography using UV light [154, 155] or e-beam lithography [156, 157], microcontact printing has received a lot of attention [86–89]. In this process, an elastomeric stamp is soaked with a solution containing the reactive molecules that should be transferred. Upon establishing conformal contact between the dried stamp and a reactive substrate, transfer of molecules takes place in those regions where contact is established. If diffusion of the ink molecules via the surface or the gas phase can be excluded, patterns of one type of molecule can be prepared. For μCP of thiols on gold, it has been shown that high-quality SAMs are formed [158] and refilling of the uncontacted (unfunctionalized) areas leads to SAMs exposing two functionalities.

The micropatterning of PAMAM dendrimers relies on μCP with a hydrophilized stamp. An UV/ozone treatment increases the surface energy of the PDMS [159, 160] and thus provides the necessary homogeneous loading of the stamp (Fig. 16). Contact mode AFM height and friction images recorded on micropatterned dendrimer surfaces show that elevated areas

with high friction can be observed after transfer of G4 PAMAM dendrimers to NHS – C10 SAMs. The friction contrast can be understood via surface energy arguments, as the dendrimers are more hydrophilic than the unmodified NHS ester surface. Preferential adsorption of water to the dendrimer regions will result in considerable capillary forces, that lead to higher friction forces.

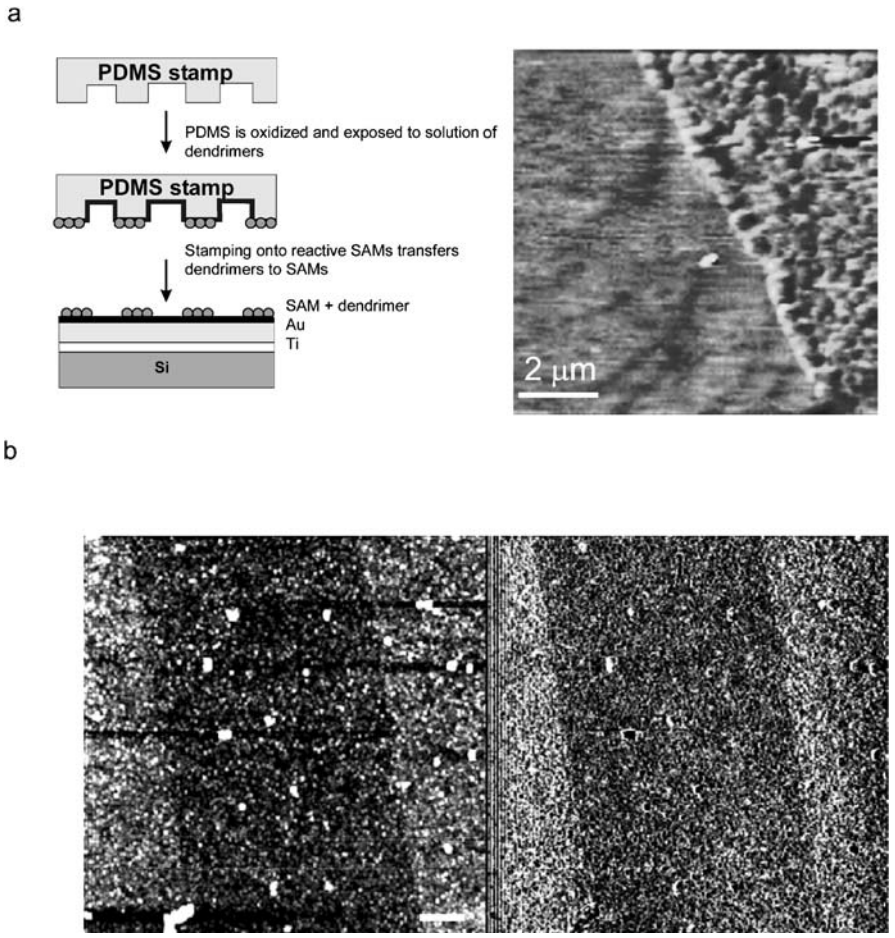

Fig. 16 **a** *Left*: Schematic of μCP process; *right*: Top view of AFM height image acquired at the border between NHS SAM and dendrimer-modified NHS SAM on an atomically flat Au(111) sample. **b** CM-AFM height and friction images of NHS – C10 SAM patterned with PAMAM G4 by microcontact printing (acquired in air; scale bar 1 μm, the height scale covers 14 nm from dark to bright; the friction forces (a.u.) increase from dark to bright contrast). In these lower resolution images obtained on granular gold, the low friction areas correspond to bare NHS – C10 SAM and the high friction areas to the immobilized dendrimers. (Reprinted in part with permission from [77], copyright (2004), American Chemical Society)

In the higher resolution image (Fig. 16a) one can discern many densely packed globular particles and only a few irregular clusters. Each of the bright spots may represent a single dendrimer molecule. The edge of the stamped area is remarkably sharp (edge roughness $\leq$ apparent width of a single dendrimer). Hence substantial surface diffusion of the dendrimers during or after printing can be ruled out. The diffusion of the "ink" is probably strongly minimized compared to low molar mass inks due to the molecular mass and the covalent attachment. Thus, in principle, higher resolution can be achieved. Our data agree with results reported by the group of Reinhoudt, who used "heavyweight" molecules [161], and by Huck and coworkers, who studied μCP with dendrimers on silicon substrates [162, 163].

The ease of μCP with dendrimers and the high level of definition of the transferred pattern indicate that μCP with this high molecular weight "ink" provides a interesting method of patterning with possibly sub-μm features. Hence, the simple and cost-effective fabrication of functionalized high definition arrays appears to be possible using microcontact printing. In the data presented, the limiting factor for the smallest attainable feature size is represented by the dimensions of the stamp.

2.2.3
Nanopatterning of Dendrimers by Scanning Probe Lithography

The patterning strategy (high molecular mass adsorbate and robust covalent attachment) can be extended to sub-100 nm sized patterns by exploiting AFM-tip assisted transfer of PAMAM dendrimers. By scanning surfaces with an AFM tip, which has been previously coated with the dendrimers, molecules can be deposited onto, say, silicon, mica or SAMs of NHS – C10. In the case of mica and oxidized silicon substrates, the originally deposited patterns were detectable, but the AFM friction images showed that dendrimer molecules may have diffused over the substrates. Based on the currently available data, spontaneous diffusion or tip-induced effects cannot be differentiated. It is, however, clear that the patterns produced do not possess sufficient stability and definition to be of any use.

By contrast, when a NHS – C10 SAM on gold was used as a substrate in DPN experiments, stable patterns were deposited, as observed in AFM friction images. By scanning an AFM tip inked with G4 PAMAM dendrimers (5.6×10^{-5} M methanolic solution) over a NHS – C10 SAM, patterns with sub-100 nm line widths could be fabricated via DPN. In Fig. 17a, a friction force AFM image of lines 2 μm long and 50 ± 20 nm wide is shown; in Fig. 17b the lines are 1 μm long and 70 ± 10 nm wide.

The observation of stable patterns underlines the importance of covalent attachment to achieve robust patterns, and it confirms the overall strategy employed. Thus, NHS – C10 SAMs can be easily and rapidly functionalized with PAMAM dendrimers via amide linkage formation in a very simple

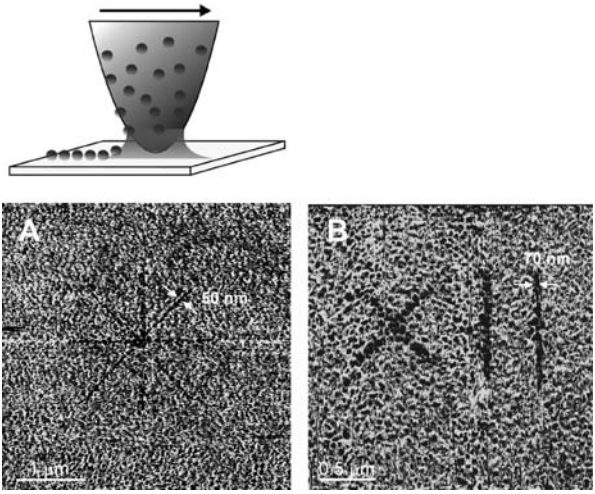

Fig. 17 *Top*: Schematic of DPN process; *bottom*: Sequence of LFM force images (acquired in air; friction forces (a.u.) increase from dark to bright contrast) of arrays of lines with mean widths (± standard deviation) of 50 ± 20 nm and 70 ± 10 nm produced by DPN of G4 PAMAM dendrimers on NHS – C10 SAMs on granular gold. The contrast in the LFM scans is reversed compared to the microcontact-printed patterns, which were scanned with a clean Si_3N_4 tip. As also observed in an independent study [92], the remaining "ink" on the AFM tip used for DPN alters the relative magnitude of the friction forces in this situation. (Reprinted with permission from [77], copyright (2004), American Chemical Society)

and straightforward process. Using μCP and DPN, micron- and sub-100 nm-scale patterns have been produced. The resolutions of the patterns obtained in our work are probably limited only by the size of the stamps and the scanned areas in DPN. Together with the demonstrated quasi-3D architecture, which allows one to achieve high molecule loading in coupling reactions for chip-based assays and sensor surfaces, these layers constitute an interesting platform for the attachment of biomolecules via exposed primary amino groups.

2.3 Nanofabrication of Patterned Biocompatible Bilayer-Vesicle Architectures

Lipid bilayers and surface immobilized vesicles provide an alternative architecture for the micro- and nanofabrication of bioreactive and biocompatible platforms [63–67]. In recent years, the modification of solid surfaces with biological molecules has been widely studied as a means to obtain biomimetic interfaces for biomedical and environmental applications. Among the various formats of functionalized interfaces investigated, substrate-supported lipid bilayers have received considerable attention. Proteins have been successfully

incorporated and shown to be functional in substrate-supported lipid bilayers [163], and the need for a water layer between bilayer and substrate in order to protect sensitive proteins from malfunction or denaturation has been realized which has prompted significant research in, for example, the area of polymer-tethered lipid membranes [63, 165, 166].

As a viable alternative, intact vesicles have been immobilized on solid supports and studied for possible applications in the area of biotechnology [167–170] and to develop chemosensors [171]. There are two main immobilization approaches: (a) immobilization via interaction of complementary DNA fragments that are exposed on the surface and the vesicle membrane, respectively [167, 168]; (b) immobilization mediated by specific streptavidin-biotin interactions [169]. These vesicle systems possess the advantage that the underlying substrate interferes only marginally or not at all with the membrane properties of the immobilized vesicles [172, 173]. Here we discuss a scanning probe lithography-based, label-free method to guide vesicle adsorption to a specific location in the substrate-supported bilayer membrane [174].

2.3.1
Bilayer Formation via Vesicle Fusion

Bilayers on surfaces, including SAM of thiols with hydroxyl end groups, can be formed by vesicle fusion [175, 176]. The process, as depicted schematically in Fig. 18, can be followed conveniently by in situ AFM measurements [177, 178]. As shown by various authors, the vesicle surface coverage, the mechanism of adsorption and bilayer formation, and the vesicle dimensions are directly accessible. Using appropriate models, the adhesion potential and the critical rupture radius of the vesicles can be calculated [179].

2.3.2
Bilayer Architectures on Patterned Supports for Biosensing

As mentioned, substrate-supported lipid bilayers are attractive systems for studying embedded proteins and constructing biosensors. For applications including molecular separation [180], lipid bilayer compartments or patterned bilayers have been utilized [66, 181, 182]. Different approaches to obtaining patterned bilayers have been described recently, including photopolymerization [183], mechanical manipulation [184–186], or the use of prepatterned supports [187–189].

A convenient strategy combines the use of prepatterned SAMs prepared by μCP and bilayer formation by vesicle fusion (Sect. 2.3.1) [164]. As shown schematically in Fig. 19, this approach comprises, in a first step, the patterning of a SAM (a cholesterol-terminated thiol is transferred to the gold substrate, the remaining areas are back-filled with the hydrophilic hydroxy-

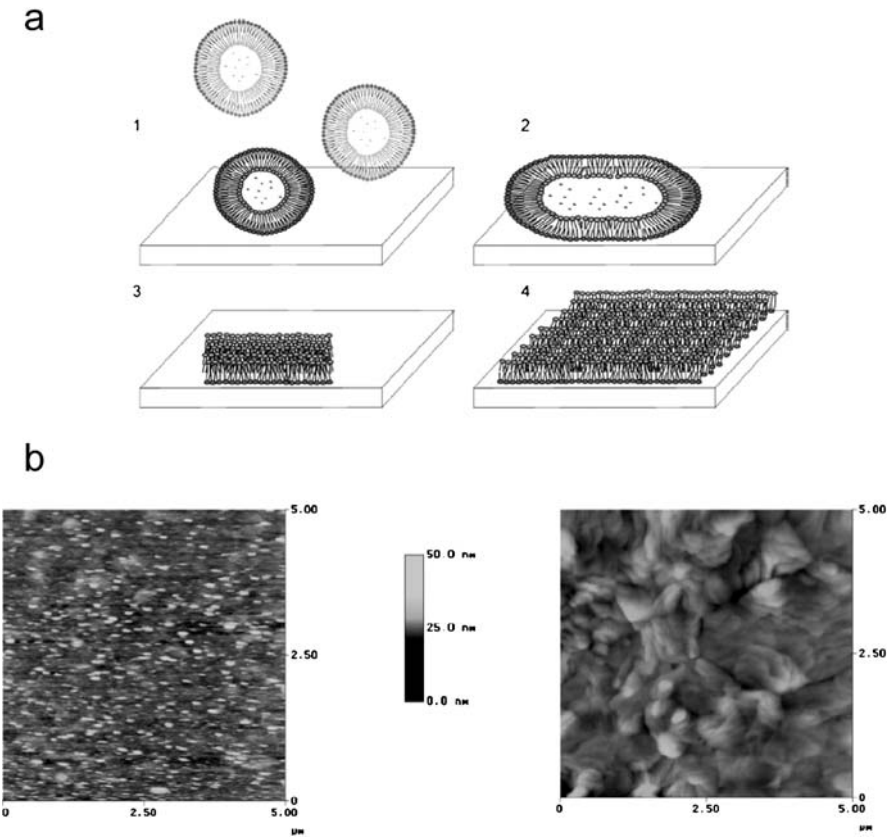

Fig. 18 **a** Four-step scenario of supported bilayer formation via vesicle fusion comprising **1** vesicle adsorption, **2** fusion of vesicles at the surface to form larger vesicles, **3** rupture of the fused vesicles resulting in bilayer discs, and finally **4** merging of the discs. **b** *Left*: AFM height image of DMPC vesicles (nominal diameter of 50 nm) adsorbed to mercaptoethanol SAM on annealed gold; *right*: AFM height image of DMPC bilayer on mercaptoethanol SAM on annealed gold at increased solution concentrations (images were acquired in buffer at minimized force)

terminated mercaptoethanol). Among the advantages of the subsequent deposition of a lipid bilayer and lipid monolayer on the hydrophilic and hydrophobic areas, respectively, are reduced leakage currents in electrochemical detection, spatial control of the in-plane bilayer architecture (size, shape, and distribution of bilayer areas), and the possibility of incorporating transmembrane proteins localized in bilayer regions in which they are adsorbed (in other words, the possibility of restricting their lateral motion) [164].

Nanometer-scale characterization of the fabricated architectures is again important. Figure 20 shows typical friction force scans of the patterned monolayer samples before and after bilayer formation. In some of the experi-

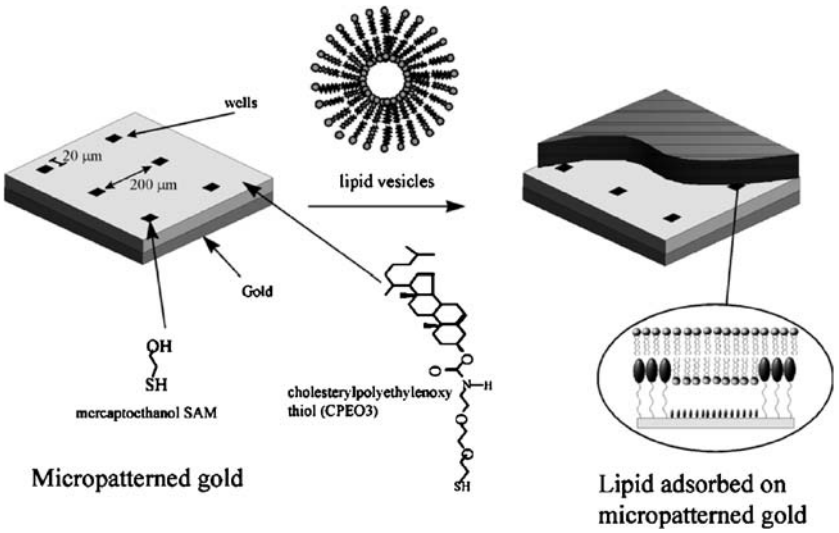

Fig. 19 Schematic drawing of bilayer deposition by vesicle fusion on patterned SAMs prepared by microcontact printing. (Reprinted with permission from [164], copyright (1999), American Chemical Society)

ments, chemical modification of gold-coated AFM tips with octadecanethiol was used to enhance the contrast in the imaging medium [142].

Prior to the unrolling of the vesicles (Fig. 20a), the friction observed in *water* on the mercaptoethanol part is *lower* than on the cholesterol part. The contrast observed is dominated by hydrophobic forces. The mercaptoethanol-functionalized parts of the sample are solvated to a much higher degree than the hydrophobic cholesterol parts [144]. The friction forces show the same trend, which indicates that the adhesion forces dominate the interaction between tip and surface in this case.

After unrolling the vesicles, the friction contrast was reversed in measurements in water (Fig. 20b). In this case the mercaptoethanol areas show *higher* friction. The observed contrast cannot be explained by different forces between tip and surface functional groups because the functional groups exposed at the surface are the *same*. However, the mechanical properties of the lipid monolayer on the more rigid CPEO3 part are different to the more fluid lipid bilayer on top of the mercaptoethanol [190]. At a given imaging force, the AFM tip penetrates more into the lipid bilayer, and so the contact area between tip and sample is increased, resulting in more pronounced energy dissipation and thus higher friction force.

Using electrochemical impedance measurements, it was demonstrated that these micropatterned thiol-terminated lipophilic SAMs can be used to support lipid membranes that meet the key criteria required for use as potential biosensors: they are integral enough (sufficiently blocking) for lipid bilayer

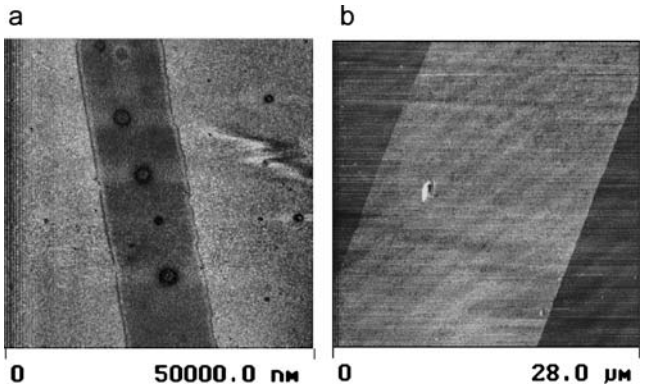

Fig. 20 **a** AFM friction force micrograph (friction forces increase from low (*dark*) to high (*bright*)) measured on patterned SAM (*stripe*: mercaptoethanol) prior to bilayer deposition. **b** Corresponding friction force micrograph acquired after bilayer formation. (Reprinted in part with permission from [164], copyright (1999), American Chemical Society)

ion channel selectivity to be observed (demonstrated for valinomycin and gramicidin A) [164]; they are formed over hydrophilic SAM regions (mercaptoethanol) and so should have a water layer under the bilayer, which is important for the addition of more complex proteins, especially large ion channels. The bilayers also appear to be relatively fluid (from comparing the frictional forces of the lipid covered cholesterol and lipid covered mercaptoethanol areas).

2.3.3 Directing Vesicle Adsorption to Bilayers by SPL

Instead of utilizing (patterned) substrate-supported membranes for protein studies, and so on, vesicles can be immobilized on suitable substrates. The adsorption of vesicles onto lipid bilayers can be spatially controlled and directed in situ, in principle, with nanometer-scale precision using an AFM-based approach [174]. This strategy enables one to fabricate patterned vesicle arrays without the need to implement molecular recognition units in the vesicles, and hence is applicable to a broad range of systems.

The strategy consists of scanning, say, a previously formed 1.2-dimyristoyl-*sn*-glycero-3-phosphatidylcholine (DMPC) bilayer on a mercaptoethanol SAMs in the presence of DMPC vesicles with an AFM tip, followed by immobilization of vesicles from solution to altered areas of the SAM-supported bilayer (Fig. 21). In the "writing step", patterns are scanned using normal forces of 30–50 nN repeatedly (the bilayer was visibly damaged for forces $> \sim$ 80–100 nN). The interaction of the tip with the bilayer leads to a local modification of the layer. This alteration presumably changes the adhesion

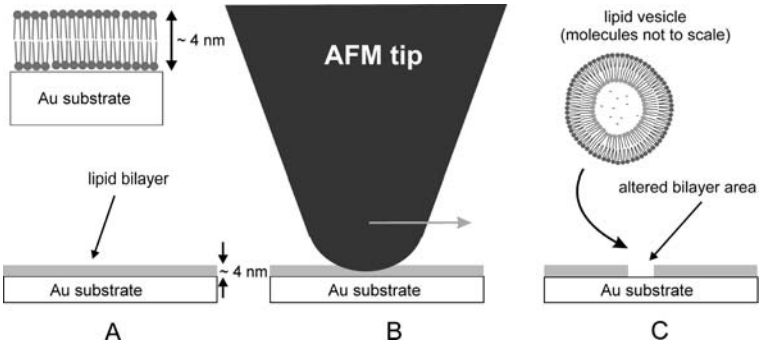

Fig. 21 Schematic of AFM tip-assisted immobilization drawn approximately to scale (bilayer thickness: ~ 4 nm; tip radius: 20 nm; vesicle diameter ~ 40 nm): **a** An intact defect-free DMPC bilayer is formed on a mercaptoethanol SAM on gold (SAM is omitted from schematic); **b** subsequent scanning with an AFM tip at high force leads to local damage of the bilayer; **c** in these areas (the schematic drawing does not imply any molecular detail concerning the damage created in step (**b**)) vesicles will adsorb from the solution and stay immobilized. (Reprinted with permission from [174], copyright (2004), American Chemical Society)

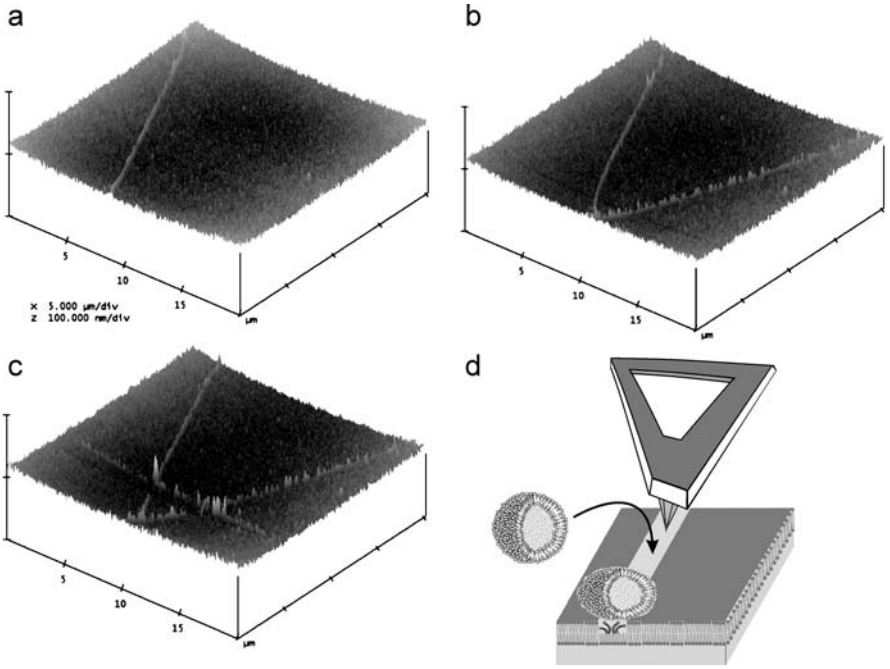

Fig. 22 The stepwise fabrication of vesicle patterns is shown in the sequence of AFM images **a**–**c** (image size: 20 μm × 20 μm). The scanning probe lithographic modification and the adsorption process of vesicles in solution onto the altered part of the bilayer is depicted schematically in **d** (no molecular-level structural details of the AFM tip-induced line are implied in the schematic)

potential [191, 192] such that vesicle adsorption is possible; in fact the deposited vesicles are much more strongly adsorbed and resist shear forces much better compared to the situation on glass or intact bilayers. As shown in Fig. 22, the resulting assembly can be imaged by contact mode AFM noninvasively using imaging forces of < 1 nN.

The stepwise nanofabrication of a vesicle pattern is shown in Fig. 22. A first line of vesicles is observed after scanning a single scan line under a load of ~ 40 nN for one minute (Fig. 22a). The next AFM images show the result of scanning a second and a third line at angles of 60° relative to the first and second line, respectively (Figs. 22b and 22c). The vesicles were found to possess similar dimensions to those adsorbed from solution onto the bare SAMs [174], so lines of *individual* vesicles were deposited.

The guided vesicle deposition is attributed to a very localized AFM tip-induced alteration of the original DMPC bilayer, which results in the adsorption of vesicles from the supernatant solution. Vesicle patterns with widths equal to the vesicle size can be fabricated over lengths exceeding 25 μm [174]. Based on an estimate of the tip–sample contact area, the line width is given by the width of the vesicle adsorbed on the bilayer.

In conclusion, this novel method of lipid vesicle immobilization on substrate-supported lipid bilayers in a spatially confined manner may serve as a platform for research on proteins incorporated in the lipid bilayers comprising the vesicles. Owing to their structural similarities to the cell membrane, lipid bilayers and substrate-immobilized vesicles provide interesting platforms for studies of incorporated proteins, an area that will see progressive growth in the near future.

3 Outlook

In this contribution, recent advances in our studies on organic and macromolecular films and assemblies for future applications as (bio)reactive platforms were briefly reviewed. Emphasis was placed on the model character of each system investigated. It is clear that these model systems may possess limitations and that system-specific peculiarities can be very important in applications, or where the coupling of specific proteins (for instance) is concerned. However, the acknowledgement of the importance of structural, conformational and compositional characterization on the relevant length scale, the close relationship between structure and reactivity for different architectures, and the possibilities for unconventional micro- and nanofabrication of reactive platforms provide a set of general guidelines that enable one to design reactive platforms in a specific context.

While highly organized monolayer approaches appear to be appealing in many ways, the limited reactivity and limited attainable surface coverages are

clear drawbacks. In fact, analysis of the results summarized in this contribution shows that, for a number of scenarios, compositionally and structurally defined yet *disordered* systems possess clear advantages. The extension from 2D to quasi-3D constitutes a generic strategy for increasing the surface coverage in coupling reactions, while stability and diffusion-related problems necessitate the crosslinking of polymeric systems in hydrogel formats [70–72, 193].

Combinations of the very simple spin-coated reactive polymer films discussed in Sect. 2.1.4 with the micro- and nanopatterning approaches studied and refined in model studies on well-defined macromolecular (dendrimer) systems are currently being investigated with substantial success. Thus, the lessons learned in these model studies can be applied to practical formats in order to provide reactive micro- and nanopatterned platforms for the development of biosensors, biochips (DNA, proteins, saccharides, and so on) and studies of cell–cell and cell–substrate interactions.

Acknowledgements The authors would like to thank Dr. Mark A. Hempenius, Dr. Kenichi Morigaki, Dr. Toby Jenkins, Prof. Dr. Stephen D. Evans, Dr. Joseph M. Johnson, Dr. Peter Lenz, Prof. Dr. Curtis W. Frank, Prof. Dr. Steven G. Boxer, Dr. Victor Chechik, and Prof. Dr. Helmut Ringsdorf for very fruitful and stimulating discussions. This work has been financially supported in part by the European Community's Human Potential Programme under contract HPRN-CT-1999-00151 (G.J.V.), the EU Socrates program (D.I.R.), the MESA$^+$ Institute for Nanotechnology of the University of Twente, the Council for Chemical Sciences of the Netherlands Organization for Scientific Research (CW-NWO) (B.D.), also in the framework of the *vernieuwingsimpuls* program (H.S., C.L.F., A.S.).

References

1. Clark JH, Macquarrie DJ (1996) Chem Soc Rev 25:303
2. Mirkin CA, Ratner MA (1992) Annu Rev Phys Chem 43:719
3. Ricco AJ, Crooks RM, Osbourn GC (1998) Acc Chem Res 31:289
4. Paolesse R, Di Natale C, Macagnano A, Davide F, Boschi T, D'Amico A (1998) Sens Actuators B Chem 47:70
5. Everhart DS (1999) Chemtech 29:30
6. Wessa T, Gopel W (1998) Fres J Anal Chem 361:239
7. Storri S, Santoni T, Minunni M, Mascini M (1998) Biosens Bioelectron 13:347
8. Wang J (1992) ACS Symp Ser 487:125
9. Allara DL (1995) Biosens Bioelectron 10:771
10. Fodor SPA, Read JL, Pirrung MC, Stryer L, Lu AT, Solas D (1991) Science 251:767
11. Schena M, Shalon D, Davis RW, Brown PO (1995) Science 270:467
12. Chee M, Yang R, Hubbell E, Berno A, Huang XC, Stern D, Winkler J, Lockhart DJ, Morris MS, Fodor SPA (1996) Science 274:610
13. Pirrung MC (2002) Angew Chem Int Ed 41:1277
14. Case MA, McLendon GL, Hu Y, Vanderlick TK, Scoles G (2003) Nano Lett 3:425
15. Liu GY, Xu S, Qian YL (2000) Acc Chem Res 33:457
16. Sigal GB, Bamdad C, Barberis A, Strominger J, Whitesides GM (1996) Anal Chem 68:490

17. Prime KL, Whitesides GM (1991) Science 252:1164
18. Jerome C, Gabriel S, Voccia S, Detrembleur C, Ignatova M, Gouttebaron R, Jerome R (2003) Chem Commun 2500
19. Tannenbaum R, Hakanson C, Zeno A, Tirrell M (2002) Langmuir 18:5592
20. Han WQ, Fan SS, Li QQ, Hu YD (1997) Science 277:1287
21. Godwin A, Hartenstein M, Muller AHE, Brocchini S (2001) Angew Chem Int Ed 40:594
22. Ulman A (1991) An introduction to ultrathin organic films: from Langmuir-Blodgett to self-assembly. Academic, New York
23. Dubois LH, Nuzzo RG (1992) Annu Rev Phys Chem 43:437
24. Ulman A (1996) Chem Rev 96:1533
25. Schreiber F (2004) J Phys Condens Matter 16:R881
26. Ferretti S, Paynter S, Russell DA, Sapsford KE, Richardson DJ (2000) Trends Anal Chem 19:530
27. Mrksich M (2000) Chem Soc Rev 29:267
28. Ostuni E, Yan L, Whitesides GM (1999) Colloids Surf B Biointerfaces 15:3
29. Schönherr H, Chechik V, Stirling CJM, Vancso GJ (2000) J Am Chem Soc 122:3679
30. Schönherr H, Chechik V, Stirling CJM, Vancso GJ (2001) ACS Symp Ser 781:36
31. Prucker O, Ruhe J (1998) Macromolecules 31:592
32. Prucker O, Ruhe J (1998) Macromolecules 31:602
33. Evans SD, Johnson SR, Ringsdorf H, Williams LM, Wolf H (1998) Langmuir 14:6436
34. Lockhart DJ, Winzeler EA (2000) Nature 405:827
35. Zhu H, Snyder M (2002) Curr Opin Cell Biol 14:173
36. Chechik V, Crooks RM, Stirling CJM (2000) Adv Mater 12:1161
37. Sullivan TP, Huck WTS (2003) Eur J Org Chem 17
38. Tollner K, PopovitzBiro R, Lahav M, Milstein D (1997) Science 278:2100
39. Neogi P, Neogi S, Stirling CJM (1993) J Chem Soc Chem Commun 1134
40. VanRyswyk H, Turtle ED, WatsonClark R, Tanzer TA, Herman TK, Chong PY, Waller PJ, Taurog AL, Wagner CE (1996) Langmuir 12:6143
41. Wang JH, Kenseth JR, Jones VW, Green JBD, McDermott MT, Porter MD (1997) J Am Chem Soc 119:12796
42. Bertilsson L, Liedberg B (1993) Langmuir 9:141
43. Su XD, Wu YJ, Robelek R, Knoll W (2005) Langmuir 21:348
44. Camillone N, Chidsey CED, Liu GY, Scoles G (1993) J Chem Phys 98:3503
45. Poirier GE (1997) Chem Rev 97:1117
46. Jaschke M, Schönherr H, Wolf H, Butt HJ, Bamberg E, Besocke MK, Ringsdorf H (1996) J Phys Chem 100:2290
47. Prime KL, Whitesides GM (1993) J Am Chem Soc 115:10714
48. Harder P, Grunze M, Dahint R, Whitesides GM, Laibinis PE (1998) J Phys Chem B 102:426
49. Lussi JW, Michel R, Reviakine I, Falconnet D, Goessl A, Csucs G, Hubbell JA, Textor M (2004) Prog Surf Sci 76:55
50. Amirgoulova EV, Groll J, Heyes CD, Ameringer T, Rocker C, Moller M, Nienhaus GU (2004) Chem Phys Chem 5:552
51. Siegers C, Biesalski M, Haag R (2004) Chem Eur J 10:2831
52. Holmlin RE, Chen XX, Chapman RG, Takayama S, Whitesides GM (2001) Langmuir 17:2841
53. Ostuni E, Chapman RG, Holmlin RE, Takayama S, Whitesides GM (2001) Langmuir 17:5605
54. Kane RS, Deschatelets P, Whitesides GM (2003) Langmuir 19:2388

55. Ostuni E, Chapman RG, Liang MN, Meluleni G, Pier G, Ingber DE, Whitesides GM (2001) Langmuir 17:6336
56. Chapman RG, Ostuni E, Liang MN, Meluleni G, Kim E, Yan L, Pier G, Warren HS, Whitesides GM (2001) Langmuir 17:1225
57. Huang NP, Michel R, Voros J, Textor M, Hofer R, Rossi A, Elbert DL, Hubbell JA, Spencer ND (2001) Langmuir 17:489
58. Ahmad J, Astin KB (1990) Langmuir 6:1797
59. Nuzzo RG, Allara DL (1983) J Am Chem Soc 105:4481
60. Sagiv J (1980) J Am Chem Soc 102:92
61. Finklea HO, Robinson LR, Blackburn A, Richter B, Allara DL, Bright T (1986) Langmuir 2:239
62. Sabatani E, Rubinstein I, Maoz R, Sagiv J (1987) Electroanal Chem 219:365
63. Ringsdorf H, Schlarb B, Venzmer J (1988) Angew Chem Int Ed 27:113
64. Sackmann E (1996) Science 271:43
65. Plant AL (1993) Langmuir 9:2764
66. Boxer SG (2000) Curr Opin Chem Biol 4:704
67. Groves JT, Boxer SG (2002) Acc Chem Res 35:149
68. Khademhosseini A, Jon S, Suh KY, Tran TNT, Eng G, Yeh J, Seong J, Langer R (2003) Adv Mater 15:1995
69. Malmqvist M, Karlsson R (1997) Curr Opin Chem Biol 1:378
70. Gehrke SH, Vaid NR, McBride JF (1998) Biotechnol Bioeng 58:416
71. Putka CS, Gehrke SH, Willis M, Stafford D, Bryant J (2002) Biotechnol Bioeng 80:139
72. Toomey R, Freidank D, Ruhe J (2004) Macromolecules 37:882
73. Niemeyer CM, Blohm D (1999) Angew Chem Int Ed 38:2865
74. Schulze A, Downward J (2001) Nat Cell Biol 3:E190
75. Benters R, Niemeyer CM, Drutschmann D, Blohm D, Wohrle D (2002) Nucleic Acids Res 30:e1
76. Pathak S, Singh AK, McElhanon JR, Dentinger PM (2004) Langmuir 20:6075
77. Degenhart GH, Dordi B, Schönherr H, Vancso GJ (2004) Langmuir 20:6216
78. Rowan B, Wheeler MA, Crooks RM (2002) Langmuir 18:9914
79. Lahann J, Balcells M, Rodon T, Lee J, Choi IS, Jensen KF, Langer R (2002) Langmuir 18:3632
80. Chen Q, Forch R, Knoll W (2004) Chem Mater 16:614
81. Zhang ZH, Chen Q, Knoll W, Foerch R, Holcomb R, Roitman D (2003) Macromolecules 36:7689
82. Zhou X, Wu L, Zhou J (2004) Langmuir 20:8877
83. Ruhe J, Golze S, Freidank D, Mohry S, Klapproth H (2001) Abstr Pap Am Chem Soc 221:U356
84. Schena M (2003) Microarray analysis. Wiley-Liss, Hoboken NJ
85. Falconnet D, Koenig A, Assi T, Textor M (2004) Adv Funct Mater 14:749
86. Kumar A, Biebuyck HA, Whitesides GM (1994) Langmuir 10:1498
87. Wilbur JL, Kumar A, Kim E, Whitesides GM (1994) Adv Mater 6:600
88. Kumar A, Whitesides GM (1994) Science 263:60
89. Xia YN, Whitesides GM (1998) Annu Rev Mater Sci 28:153
90. Ginger DS, Zhang H, Mirkin CA (2004) Angew Chem Int Ed 43:30
91. Wouters D, Schubert US (2004) Angew Chem Int Ed 43:2480
92. Auletta T, Dordi B, Mulder A, Sartori A, Onclin S, Bruinink CM, Peter M, Nijhuis CA, Beijleveld H, Schönherr H, Vancso GJ, Casnati A, Ungaro R, Ravoo BJ, Huskens J, Reinhoudt DN (2004) Angew Chem Int Ed 43:369
93. Morigaki K, Schönherr H, Frank CW, Knoll W (2003) Langmuir 19:6994

94. Chechik V, Stirling CJM (1998) Langmuir 14:99
95. Chechik V, Stirling CJM (1997) Langmuir 13:6354
96. Creager SE, Clarke J (1994) Langmuir 10:3675
97. Chatelier RC, Drummond CJ, Chan DYC, Vasic ZR, Gengenbach TR, Griesser HJ (1995) Langmuir 11:4122
98. Lee TR, Carey RI, Biebuyck HA, Whitesides GM (1994) Langmuir 10:741
99. Bain CD, Whitesides GM (1989) Langmuir 5:1370
100. Hu K, Bard AJ (1997) Langmuir 13:5114
101. Schönherr H, Hruska Z, Vancso GJ (2000) Macromolecules 33:4532
102. Schönherr H, van Os MT, Förch R, Timmons RB, Knoll W, Vancso GJ (2000) Chem Mater 12:3689
103. Israelachvili JN (1991) Intermolecular and surface forces, 2nd edn. Academic, London
104. Wirth MJ (ed) (1999) Chem Rev 99(10):2843–3152 (special issue)
105. Vancso GJ, Hillborg H, Schönherr H (2005) Adv Polym Sci 182:55
106. Ulman A (ed) (1995) Characterization of organic thin films. Butterworth-Heinemann
107. Overney RM, Meyer E, Frommer J, Brodbeck D, Luthi R, Howald L, Guntherodt HJ, Fujihira M, Takano H, Gotoh Y (1992) Nature 359:133
108. Carpick RW, Salmeron M (1997) Chem Rev 97:1163
109. Nisman R, Smith P, Vancso GJ (1994) Langmuir 10:1667
110. Schönherr H, Vancso GJ (1997) Macromolecules 30:6391
111. Vancso GJ, Schönherr H (1999) In: Tsukruk VV, Wahl KJ (eds) Microstructure and microtribology of polymer surfaces (ACS Symp Ser vol 741). American Chemical Society, New York, p 317
112. Vancso GJ, Snétivy D, Schönherr H (1998) In: Ratner BD, Tsukruk VV (eds) Scanning probe microscopy of polymers (ACS Symp Ser vol 694). American Chemical Society, New York, p 67
113. Schönherr H, Kenis PJA, Engbersen JFJ, Harkema S, Hulst R, Reinhoudt DN, Vancso GJ (1998) Langmuir 14:2801
114. Mizes HA, Loh KG, Miller RJD, Ahuja SK, Grabowski EF (1991) Appl Phys Lett 59:2901
115. Joyce SA, Houston JE, Michalske TA (1992) Appl Phys Lett 60:1175
116. Van der Werf KO, Putman CAJ, De Grooth BG, Greve J (1994) Appl Phys Lett 65:1195
117. Baselt DR, Baldeschwieler JD (1994) J Appl Phys 76:33
118. Berger CEH, Van der Werf KO, Kooyman RPH, De Grooth BG, Greve J (1995) Langmuir 11:4188
119. Radmacher M, Cleveland JP, Fritz M, Hansma HG, Hansma PK (1994) Appl Surf Sci 66:2159
120. Schmidt P, Kolarik J, Lednicky F, Dybal J, Lagaron JM, Pastor JM (2000) Polymer 41:4267
121. Benninghoven A (1994) Angew Chem Int Ed 33:1023
122. Yang ZP, Belu AM, Liebmann-Vinson A, Sugg H, Chilkoti A (2000) Langmuir 16:7482
123. Stoeckli M, Farmer TB, Caprioli RM (1999) J Am Soc Mass Spectrom 10:67
124. Fulghum JE (1999) J Electron Spectrosc Relat Phenom 100:331
125. Turner NH, Schreifels JA (2000) Anal Chem 72:99R
126. DeAro JA, Weston KD, Buratto SK, Lemmer U (1997) Chem Phys Lett 277:532
127. Dordi B, Schönherr H, Vancso GJ (2003) Langmuir 19:5780
128. Schönherr H, Feng CL, Shovsky A (2003) Langmuir 19:10843
129. Frey BL, Corn RM (1996) Anal Chem 68:3187

130. Lahiri J, Isaacs L, Tien J, Whitesides GM (1999) Anal Chem 71:777 (and references therein)
131. Wagner P, Kernen P, Hegner M, Ungewickell E, Semenza G (1994) FEBS Lett 356:267
132. Wagner P, Hegner M, Kernen P, Zaugg F, Semenza G (1996) Biophys J 70:135
133. Wojtyk JTC, Morin KA, Boukherroub R, Wayner DDM (2002) Langmuir 18:6081
134. Porter MD, Bright TB, Allara DL, Chidsey CED (1987) J Am Chem Soc 109:3559
135. Duhachek SD, Kenseth JR, Casale GP, Small GJ, Porter MD, Jankowiak R (2000) Anal Chem 72:3709
136. Cassie ABD (1948) Discuss Faraday Soc 3:11
137. Cline GW, Hanna SB (1988) J Org Chem 53:3583
138. Dordi B, Pickering JP, Schönherr H, Vancso GJ (2004) Eur Polym J 40:939
139. Dordi B, Pickering JP, Schönherr H, Vancso GJ (2004) Surf Sci 570:57
140. Frutos AG, Brockman JM, Corn RM (2000) Langmuir 16:2192
141. Delamarche E, Michel B, Gerber C, Anselmetti D, Guntherodt HJ, Wolf H, Ringsdorf H (1994) Langmuir 10:2869
142. Frisbie CD, Rozsnyai LF, Noy A, Wrighton MS, Lieber CM (1994) Science 265:2071
143. Noy A, Vezenov DV, Lieber CM (1997) Annu Rev Mater Sci 27:381
144. Sinniah SK, Steel AB, Miller CJ, ReuttRobey JE (1996) J Am Chem Soc 118:8925
145. Johnson KL, Kendall K, Roberts AD (1971) Proc R Soc Lond A 324:301
146. Stevens F, Lo YS, Harris JM, Beebe TP (1999) Langmuir 15:207
147. Wilbur J, Whitesides GM (1999) In: G Timp (ed) Nanotechnology. Springer, Berlin Heidelberg New York, p 339
148. Laibinis PE, Bain CD, Nuzzo RG, Whitesides GM (1995) J Phys Chem 99:7663
149. Spinke J, Liley M, Schmitt FJ, Guder HJ, Angermaier L, Knoll W (1993) J Chem Phys 99:7012
150. Benters R, Niemeyer CM, Wohrle D (2001) Chembiochem 2:686
151. Lackowski WM, Campbell JK, Edwards G, Chechik V, Crooks RM (1999) Langmuir 15:7632
152. Smith RK, Lewis PA, Weiss PS (2004) Prog Surf Sci 75:1
153. Yan L, Huck WTS, Whitesides GM (2004) J Macromol Sci Polym Rev C44:175
154. Tarlov MJ, Burgess DRF, Gillen G (1993) J Am Chem Soc 115:5305
155. Huang JY, Dahlgren DA, Hemminger JC (1994) Langmuir 10:626
156. David C, Muller HU, Volkel B, Grunze M (1996) Microelectron Eng 30:57
157. Mendes PM, Preece JA (2004) Curr Opin Colloid Interf Sci 9:236
158. Larsen NB, Biebuyck H, Delamarche E, Michel B (1997) J Am Chem Soc 119:3017
159. Hillborg H, Gedde UW (1998) Polymer 39:1991
160. Hillborg H, Tomczak N, Olah A, Schönherr H, Vancso GJ (2004) Langmuir 20:785
161. Liebau M, Huskens J, Reinhoudt DN (2001) Adv Funct Mater 11:147
162. Li HW, Kang DJ, Blamire MG, Huck WTS (2002) Nano Lett 2:347
163. Li HW, Muir BVO, Fichet G, Huck WTS (2003) Langmuir 19:1963
164. Jenkins ATA, Boden N, Bushby RJ, Evans SD, Knowles PF, Miles RE, Ogier SD, Schönherr H, Vancso GJ (1999) J Am Chem Soc 121:5274
165. Beyer D, Elender G, Knoll W, Kuhner M, Maus S, Ringsdorf H, Sackmann E (1996) Angew Chem Int Ed 35:1682
166. Heibel C, Maus S, Knoll W, Rühe J (1998) ACS Symp Ser 695:104
167. Yoshina-Ishii C, Boxer SG (2003) J Am Chem Soc 125:3696
168. Svedhem S, Pfeiffer I, Larsson C, Wingren C, Borrebaeck C, Hook F (2003) Chembiochem 4:339
169. Jung LS, Shumaker-Parry JS, Campbell CT, Yee SS, Gelb MH (2000) J Am Chem Soc 122:4177

170. Stamou D, Duschl C, Delamarche E, Vogel H (2003) Angew Chem Int Ed 42:5580
171. Kim JM, Ji EK, Woo SM, Lee HW, Ahn DJ (2003) Adv Mater 15:1118
172. Boukobza E, Sonnenfeld A, Haran G (2001) J Phys Chem B 105:12165
173. Stanish I, Santos JP, Singh A (2001) J Am Chem Soc 123:1008
174. Schönherr H, Rozkiewicz DI, Vancso GJ (2004) Langmuir 20:7308
175. Watts TH, Brian AA, Kappler JW, Marrack P, McConnell HM (1984) Proc Natl Acad Sci USA 81:7564
176. Watts TH, Gaub HE, McConnell HM (1986) Nature 320:179
177. Reviakine I, Brisson A (2000) Langmuir 16:1806
178. Kumar S, Hoh JH (2000) Langmuir 16:9936
179. Schönherr H, Johnson JM, Lenz P, Frank CW, Boxer SG (2004) Langmuir 20:11600
180. van Oudenaarden A, Boxer SG (1999) Science 285:1046
181. Kung LA, Kam L, Hovis JS, Boxer SG (2000) Langmuir 16:6773
182. Groves JT, Boxer SG (2002) Acc Chem Res 35:149
183. Morigaki K, Baumgart T, Offenhausser A, Knoll W (2001) Angew Chem Int Ed 40:172
184. Cremer PS, Groves JT, Kung LA, Boxer SG (1999) Langmuir 15:3893
185. Hovis JS, Boxer SG (2000) Langmuir 16:894
186. Hovis JS, Boxer SG (2001) Langmuir 17:3400
187. Groves JT, Ulman N, Boxer SG (1997) Science 275:651
188. Jenkins ATA, Bushby RJ, Evans SD, Knoll W, Offenhausser A, Ogier SD (2002) Langmuir 18:3176
189. Cremer PS, Yang TL (1999) J Am Chem Soc 121:8130
190. Dufrene YF, Barger WR, Green JBD, Lee GU (1997) Langmuir 13:4779
191. Lipowsky R, Seifert U (1991) Mol Cryst Liq Cryst 202:17
192. Seifert U (1997) Adv Phys 46:13
193. Gong P, Grainger DW (2004) Surf Sci 570:67 (and references therein)